UTILIZING CHANNEL STATE INFORMATION FOR ENHANCEMENT OF WIRELESS COMMUNICATION SYSTEMS

By

Abdorreza Heidari

A thesis
presented to the University of Waterloo
in fulfillment of the
thesis requirement for the degree of
Doctor of Philosophy
in
Electrical and Computer Engineering

Waterloo, Ontario, Canada, 2007

I hereby declare that I am the sole author of this thesis. This is a true copy of the thesis, including any required final revisions, as accepted by my examiners.

I understand that my thesis may be made electronically available to the public.

Abstract

One of the fundamental limitations of mobile radio communications is their time-varying fading channel. This thesis addresses the efficient use of channel state information to improve the communication systems, with a particular emphasis on practical issues such as compatibility with the existing wireless systems and low complexity implementation.

The closed-loop transmit diversity technique is used to improve the performance of the downlink channel in MIMO communication systems. For example, the WCDMA standard endorsed by 3GPP adopts a mode of downlink closed-loop scheme based on partial channel state information known as mode 1 of 3GPP [1]. Channel state information is fed back from the mobile unit to the base station through a low-rate uncoded feedback bit stream. In these closed-loop systems, feedback error and feedback delay, as well as the sub-optimum reconstruction of the quantized feedback data, are the usual sources of deficiency.

In this thesis, we address the efficient reconstruction of the beamforming weights in the presence of the feedback imperfections, by exploiting the residual redundancies in the feedback stream. We propose a number of algorithms for reconstruction of beamforming weights at the base-station, with the constraint of a constant transmit power. The issue of the decoding at the receiver is also addressed. In one of the proposed algorithms, channel fading prediction is utilized to combat the feedback delay. We introduce the concept of Blind Antenna Verification which can substitute the conventional Antenna Weight Verification process without the need for any training

data. The closed-loop mode 1 of 3GPP is used as a benchmark, and the performance is examined within a WCDMA simulation framework. It is demonstrated that the proposed algorithms have substantial gain over the conventional method at all mobile speeds, and are suitable for the implementation in practice. The proposed approach is applicable to other closed-loop schemes as well.

The problem of (long-range) prediction of the fading channel is also considered, which is a key element for many fading-compensation techniques. A linear approach, usually used to model the time evolution of the fading process, does not perform well for long-range prediction applications. We propose an adaptive algorithm using a state-space approach for the fading process based on the sum-sinusoidal model. Also to enhance the widely-used linear approach, we propose a tracking method for a multi-step linear predictor. Comparing the two methods in our simulations shows that the proposed algorithm significantly outperforms the linear method, for both stationary and non-stationary fading processes, especially for long-range predictions. The robust structure, as well as the reasonable computational complexity, makes the proposed algorithm appealing for practical applications.

Acknowledgements

I would like to thank my supervisor, Professor Amir K. Khandani for his valuable suggestions, supports, and guidance throughout the course of my graduate studies at the University of Waterloo.

I am also thankful to Dr. Farshad Lahouti for providing the opportunity of our joint work through the early years of my research.

I am thankful to Derek McAvoy for serving as a colleague and a valuable contact with Bell Canada, while I was doing internship at Bell Mobility in Mississauga, and afterwards. I am also thankful to him and a number of other Bell Canada employees for providing the possibility of filing our patent application in Canada and the United States.

I also wish to thank the members of my dissertation committee, Professors Elvino S. Sousa, Sue Ann Campbell, Raafat Mansour, and Murat Uysal. I express my appreciation to the organizations that funded this research. This work is funded by the Natural Sciences and Engineering Research Council of Canada (NSERC), Nortel Networks, Bell Canada, Ontario Centres of Excellence(OCE), Communications and Information Technology Ontario (CITO), and the University of Waterloo.

I am thankful to all my friends. Thanks to my friends at the University of Waterloo, especially my friends at the CST lab, who helped create a pleasant and supportive environment during my stay in Waterloo. In addition, I thank all the staff of the department of electrical and computer engineering. I am indebted to my family, and especially to my lovely wife Fatemeh, for their patience and love throughout these years. I could not have achieved this without their unlimited support.

To my loved ones

Table of Contents

List of Tables

List of Figures

Chapter 1

Introduction

1.1 Background

The challenge for the new generation of mobile radio systems is no longer to connect two parties for a conversation, but rather to provide various types of wireless services such as voice, data, and multimedia. This requires transmission of large quantities of data in densely-populated wireless and mobile networks. A much higher spectral efficiency is therefore needed because of the bandwidth limitations. Multiple antenna techniques, which are used in the Third (3G) and the Fourth Generation (4G) of communication systems, are known to enhance the capacity and the quality of the wireless communication by exploiting the available spatial diversity [2].

One of the fundamental limitations of mobile radio communications is their time-varying channel fading, which results in dramatic fluctuations in the received signal power. The traditional wireless systems are usually designed to provide good transmission quality for the worst channel conditions, leading to inefficient utilization of the channel capacity. If the receiving conditions for the users are somehow known in advance, then adaptive methods can be used to increase the spectral efficiency.

By the growing use of multi antenna systems and their need for higher spectral efficiency, adaptive transmission methods can be considered as the heart of the emerging communication systems.

The Third Generation of mobile communications is intended to increase the system performance, which is required to meet the rising demand for internet and wireless services. In particular, the 3rd Generation Partnership Project (3GPP) [3] and the 3rd Generation Partnership Project Two (3GPP2) [4] have developed the Wideband Code-Division Multiple Access (WCDMA) [5] and CDMA2000, respectively. The improvement of the downlink capacity is one of the main challenges of the 3G systems because many of the proposed services are expected to be downlink-intensive. Therefore, the *closed-loop transmit diversity* technique has been considered which is typically suitable for downlink applications [6].

The closed-loop transmit diversity technique is used to improve the performance of the downlink channel in multi-input multi-output (MIMO) communication systems. The closed-loop scheme uses partial Channel State Information (CSI) which is fed back from the mobile unit to the base station through a low-rate (and usually) uncoded feedback bit stream. There are three major imperfections which affect the closed-loop systems [7]: *feedback delay*, *feedback error*, and *sub-optimal reconstruction*:

- Feedback delay has been shown to drastically affect the performance of closed-loop systems [8, 9] as the transmitter has to use outdated CSI. This problem gets worse as the mobile speed increases because the channel is changing more rapidly.

- A closed-loop scheme is sensitive to the errors in the feedback channel [10, 11,

12]. Other than decreasing the closed-loop gain, feedback error causes another more serious problem. For decoding purposes, the receiver needs to know exactly what weights have been applied at the transmit antennas. However, the receiver is not normally aware of the location of the errors in the feedback channel, which causes mismatch at the receiver. To mitigate this problem in practice, an *Antenna-weight Verification* algorithm [13, 1] is applied which needs some extra training data at the receiver for each user.

- The reconstruction schemes used in closed-loop systems are usually not optimal due to simplifications of the algorithms, and ignoring the feedback error and delay.

These imperfections diminish the performance of closed-loop systems and must be properly addressed to provide the possibility for the efficient use of the appealing closed-loop techniques in practice.

Channel fading prediction can be used to improve the performance of telecommunication systems in various ways. Prediction of the rapidly changing fading envelope of a mobile radio channel enables a number of capacity improving techniques like resource allocation and link adaptation. Having estimates of future samples of the fading coefficients enhances the performance of many tasks at the receiver and/or at the transmitter, including adaptive coding and modulation, channel equalization, the decoding process of data symbols, and antenna beamforming. In particular, the performance of adaptive coding and modulation techniques strongly depends on the performance of the fading prediction algorithm [14], and usually a long-range prediction algorithm is required [15]. Another application of the fading prediction is to

compensate for the effect of feedback delay in closed-loop communication systems [16], as is addressed in chapter 3. An extensive literature survey on the subject of fading modeling and prediction can be found in [15].

The time-varying mobile fading channel can be estimated from the received data to obtain observation samples of the impulse response of the channel. These observations are then used to predict the future samples of the channel fading. The most widely used mobile fading model, called Jakes model [17], and its derivatives are based on the correlation properties of the fading signal. This model works for the rich scattering environments and could be properly utilized by linear prediction, e.g. using auto-regressive (AR) models. But a practical fading model is made of a few scatters [18] in many environments, and also the stationarity assumption of Jakes model is no longer valid in time-varying systems. Therefore, we focus on a non-stationary fading model, namely the sum-sinusoid model [19, 15]. This model can capture the time-varying properties of the fading signal, and is developed based on the mechanism of signal scattering in a mobile environment.

1.2 Summary of the Dissertation

Chapter 2 addresses the efficient reconstruction of the beamforming weights in the presence of feedback error, with the constraint of a constant transmit power. In this research, some joint source-channel coding (JSCC) techniques are adopted to improve the performance of the feedback-utilized beamforming schemes by taking advantage of the residual redundancy available in the quantized channel state information. By using MAP (Maximum A Posteriori) and MMSE (Minimum Mean Square Error) approaches, we propose a number of algorithms for reconstruction of beamforming weights at the base station for the closed-loop mode 1 of the 3GPP standard. Of course the proposed approach could be used for the enhancement of any closed-loop communication system which uses quantized channel feedback.

Chapter 3 also considers the issue of feedback delay, and proposes two approaches to improve the performance. One is based on using a channel predictor at the receiver to compensate for the delay, and using the method proposed in chapter 2 to compensate for the feedback error. Another approach deals with both feedback error and delay in a unified reconstruction algorithm using JSCC techniques, by taking advantage of the redundancy available in the stream of the channel state information. Furthermore, we introduce the concept of Blind Antenna Verification which can substitute for the conventional Antenna Weight Verification process without the need for any training data. This concept is used in a joint beamforming and antenna verification algorithm which addresses the problem of beamforming and decoding in a closed-loop system. It is demonstrated that the proposed algorithms outperform the conventional methods at all mobile speeds, regardless of the quality of channel estimation. The structure of the proposed methods is suitable to be used in practical

mobile radio systems, and particularly can be considered as a contribution to the 3GPP standard.

Chapter 4 addresses the problems of modeling and prediction for fading channels. First, a multi-step predictor is presented for a popular linear approach. Then a tracking algorithm for coefficients of the multi-step linear predictor is proposed. In the next parts, a new approach is introduced. Based on the sum-sinusoidal fading model, a state-space method is proposed and is utilized to construct an adaptive Kalman filter. For updating the doppler frequencies, an acquisition-tracking approach is applied. Furthermore, a progressive forecasting method is used for the multi-step prediction of the state vector. The simulations compare the two fading prediction methods, for both Jakes fading and the generated time-varying fading. It is shown that the performance difference is significant, especially at high mobile speeds and for long-range predictions.

Chapter 2

Feedback Error in Closed-loop Wireless Systems

The closed-loop transmit diversity technique is used to improve the performance of the downlink channel in MIMO communication systems. The WCDMA standard endorsed by 3GPP adopts a mode of downlink closed-loop scheme based on partial channel state information known as mode 1. The information is fed back from the mobile unit to the base station through a low-rate uncoded feedback bit stream. In this chapter, several reconstruction techniques are introduced to improve the performance of mode 1 of 3GPP in the presence of feedback error, by taking advantage of the redundancy available in the bitstream of channel state information. We propose a number of algorithms for reconstruction of beamforming weights at the base-station, with the constraint of a constant transmit power. The performance is examined within a simulated WCDMA framework. It is demonstrated that the proposed algorithms have substantial gain over the conventional method for low, moderate and high mobile speeds. It is also shown that the proposed algorithms can substitute for the Antenna Weight Verification process done at the mobile unit in some cases. The proposed approach is applicable to other feedback schemes as well.

2.1 Introduction

Transmit diversity techniques are widely used for high-demand downlink applications [6]. Transmit diversity can be used with or without using Channel State Information (CSI) at the transmitter, which is called *closed-loop* or *open-loop*, respectively. In the 3G evolution, open-loop techniques such as Orthogonal Transmit Diversity [6] and Space-Time Transmit Diversity [20], and closed-loop techniques such as Switched Transmit Diversity and *beamforming* (also called Transmit Adaptive Array) [6] have been considered. 3GPP has included Alamouti Space-Time Coding [21], and one beamforming mode as parts of the FDD (Frequency Division Duplex) WCDMA downlink system [1]. Generally speaking, open-loop schemes are more robust as they do not need any CSI, whereas closed-loop schemes provide a higher capacity which is needed for the new services. Closed-loop schemes are known to be effective for low-speed mobile users, but fail at high mobile speeds [6].

A beamforming scheme enables the transmit array to beamform the transmit signal according to a particular channel state. In a MIMO system, when there is adequate CSI available at the transmitter, beamforming strategy is optimal in terms of the system capacity [22]. With beamforming, the transmissions from different antenna elements at the base station add constructively at the receiver, improving the received SNR. However, this improvement requires that the transmitter has a fairly accurate knowledge of the parameters of the channel to the intended receiver. This is difficult to achieve as these parameters are time-varying. Furthermore, in a practical communication system, feedback data is subject to imperfections such as quantization noise [23], feedback error [23, 10] and feedback delay [24]. Maintaining the closed-loop performance by using the available imperfect feedback data is an

important issue for practical systems.

This chapter presents methods to mitigate the problems of the closed-loop mode 1 of 3GPP in the presence of feedback error, and to improve the performance of the underlying weight reconstruction algorithm. There are few studies that address the problems of the closed-loop mode of the 3GPP standard, e.g. [25]. Here, we propose an approach to enhance the performance of mode 1 of 3GPP at different mobile speeds. Our approach is applicable to other closed-loop schemes similarly. It is shown that the proposed algorithms result in substantial savings in the base-station transmit power in comparison with the suggested reconstruction scheme for mode 1 in the 3GPP standard. The algorithms are compatible with the current standard framework, and they are appropriate for the practical mobile systems in terms of robustness and complexity. Our assumptions and simulation parameters are consistent with the FDD WCDMA closed-loop mode.

The structure of the rest of this chapter is as follows: Section 2.2 includes a general description of a closed-loop system, as well as our notations and channel model. In Section 2.2.2, some conventional channel feedback schemes are examined, and Section 2.2.6 introduces our feedback model. Section 2.3 describes the algorithm of mode 1 of the 3GPP standard, and its problems and challenges in the presence of feedback error. Section 2.5 explains our approach to reconstruct the beamforming weights, and elaborates on the proposed methods and algorithms. Finally, Section 2.6 shows the simulation results and compares the performance of our proposed algorithms with the conventional methods in various conditions. Here is a list of notations used in this chapter (and the next one): $[\cdot]^{(k)}$ refers to the k'th element of a vector, $[\cdot]^H$ is the Hermitian transform, and $\mathbb{C}$ is the set of complex numbers.

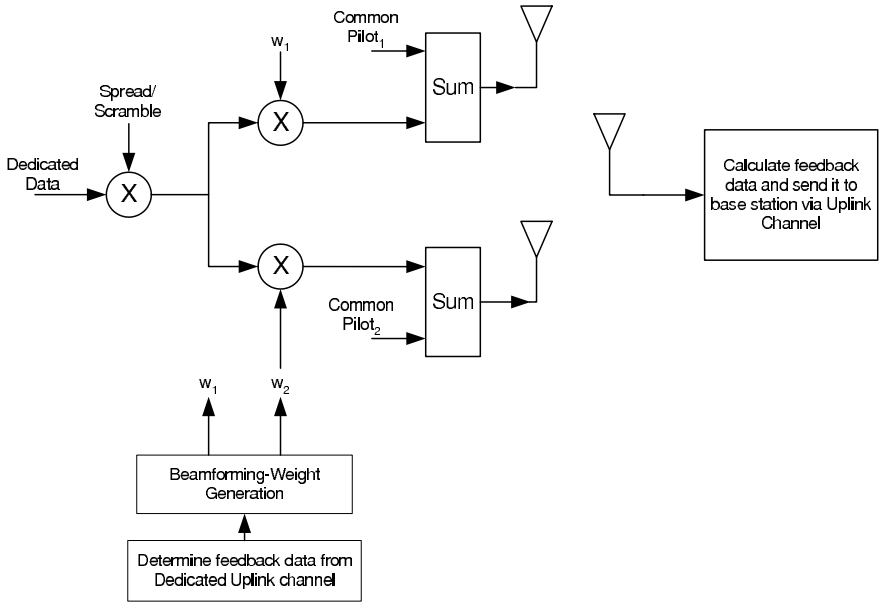

Figure 2.1: Closed-loop mode of a 3GPP system

2.2 Closed-loop Systems

Figure 2.1 shows a functional diagram of the closed-loop modes[1] of the downlink 3GPP standard [1]. A general description of the feedback system follows. After the channel is estimated in the receiver by using the transmitted pilots, the CSI is quantized and sent back to the transmitter. The transmitter computes the required beamforming coefficients and applies them to the transmit antennas. In practice, the feedback channel has a low rate. Furthermore, there is delay and potential errors in the feedback channel. In spite of these imperfections in the feedback data, the closed-loop schemes perform significantly better than the open-loop schemes at low mobile speeds [6].

[1]Namely, mode 1 and mode 2. Mode 2 is no longer part of the 3GPP standard.

Consider a system with M transmit antennas and one receive antenna. A flat fading channel is considered from each transmit antenna to the receive antenna. Dropping the time indices for simplicity, we write

$$r = \mathbf{h}^T \mathbf{x} + \eta, \tag{2.1}$$

where r is the received signal at the receiver,

$$\mathbf{h} = [h^{(1)} \cdots h^{(M)}]^T \in \mathbb{C}^M \tag{2.2}$$

is the channel coefficients complex vector, where $h^{(m)}$ represents the channel between the m-th transmit antenna and the receive antenna,

$$\mathbf{x} = [x^{(1)} \cdots x^{(M)}]^T \in \mathbb{C}^M \tag{2.3}$$

represents the channel input vector. η is a complex circularly symmetric AWGN (Additive White Gaussian Noise) with the variance N_0, $\eta \sim \mathcal{N}(0, N_0)$. There is a constraint on the total transmit power, $E[\|\mathbf{x}\|^2] = \sum_{m=1}^{M} E[\left|x^{(m)}\right|^2] \leq M$.

2.2.1 Channel Model

For the channel model, we consider a Rayleigh fading model, and so $h^{(m)}, m = 1, \cdots, M$, are zero-mean independent, identically distributed, circularly symmetric Gaussian random variables. Each coefficient is expressed as

$$h^{(m)} = \alpha^{(m)} e^{j\phi^{(m)}}, \tag{2.4}$$

where $\alpha^{(m)}$ and $\phi^{(m)}$ are the amplitude and the phase, respectively. It is well-known that $\alpha^{(m)}$ has a Rayleigh distribution [26]

$$p(\alpha^{(m)} = a) = a\, e^{-a^2/2}, \qquad a \geq 0 \tag{2.5}$$

and $\phi^{(m)}$ has a uniform distribution,

$$p(\phi^{(m)} = \theta) = \frac{1}{2\,\pi}, \qquad 0 \leq \theta < 2\,\pi. \tag{2.6}$$

It is also known that the autocorrelation function of the fading for the two-dimensional isotropic scattering and an omni-directional receiving antenna is given by [27]

$$R(t, t-\delta) = \frac{E[h(t)h^*(t-\delta)]}{\sigma_h^2} = J_0(2\pi f_d \delta), \tag{2.7}$$

where σ_h^2 is the fading power, $J_0(\cdot)$ is the first-kind Bessel function of the zero order, f_d is the doppler frequency, and δ is the time difference.

The Jakes fading generator [17], which is a popular simulator for mobile fading channels, has been proposed based on the properties given in (2.5-2.7). It utilizes a number of low-frequency oscillators to generate a fading signal for a given mobile speed. The original Jakes model generates a non-stationary signal. For the simulations, we use a modified Jakes fading generator suggested in [27] to generate a stationary signal.

In our analysis in this chapter, we assume that all the elements of the channel vector $\mathbf{h}$ are known at the receiver. This assumption allows for a better comparison between different schemes in the presence of feedback error, regardless of the channel estimation errors. It is noteworthy that in the 3GPP systems, there is a separate Common Pilot Channel (CPICH), with a relatively large proportion of the base station power, which allows each receiver to accurately estimate its channel coefficients [13], and this supports the above assumption.

2.2.2 Beamforming

In a closed-loop system, channel input $\mathbf{x}$ should be appropriately selected according to the channel state [28]. Controlling the channel input can be accomplished with a conventional beamformer which applies some weights to the transmitted signal for each antenna. Assuming two transmit antennas and one receive antenna, a beamforming scheme can be expressed as

$$\mathbf{x} = \mathbf{w}s, \tag{2.8}$$

where

$$\mathbf{w} = [w^{(1)}, w^{(2)}]^T \in \mathbb{C}^2, \tag{2.9}$$

and s is the transmitted symbol. It is assumed that $\|\mathbf{w}\|^2 = 1$, which means the beamformer does not change the transmit power.

2.2.3 Decoding at the Receiver

The received signal r is a complex number which is the superposition of the signals from different antennas, as well as the noise, i.e.,

$$\begin{aligned} r &= \mathbf{h}^T\mathbf{w}s + \eta & (2.10)\\ &= (\sum_{m=1}^{2} h^{(m)}w^{(m)})s + \eta. & (2.11) \end{aligned}$$

In the decoding process at the receiver, the combining weight $v \in \mathbb{C}$ is applied as [26]

$$z = v^H r = v^H\mathbf{h}^T\mathbf{w}s + v^H\eta, \tag{2.12}$$

where z is used to calculate the output LLR (Log-Likelihood Ratio) values (refer to [29] for further information on different combining schemes in WCDMA). It has been

shown [30] that to minimize the average probability of error in a MIMO system (and therefore in a MISO system like ours), $\mathbf{w}$ and v should be jointly selected to maximize the instantaneous SNR. Noting (2.12), we have

$$\mathrm{SNR}_{inst} = \left|\mathbf{h}^T\mathbf{w}\right|^2 \frac{E_s}{N_0} \tag{2.13}$$

where $E_s = E[|s|^2]$. It is observed that the SNR does not depend on v in the case that there is one receive antenna (the case considered in the current work).

For the selection of $\mathbf{w}$, several schemes are introduced in the literature, for example refer to [28]. A number of conventional schemes to select $\mathbf{w}$ are given in the next sections. As will be shown later, the accuracy in the calculation of v plays an important role in the overall system performance. To address this problem, conventionally an Antenna Weight Verification algorithm is utilized which is explained in Section 2.4.1. Specifically, we will tackle this issue in the next chapter, and introduce a novel blind method in Section 3.3.1.

2.2.4 Ideal Feedback

Maximizing the instantaneous SNR in (2.13), the optimum weights are found as

$$\mathbf{w}^{ideal} = \arg\max_{\mathbf{w}} \left|\mathbf{h}^T\mathbf{w}\right|^2, \tag{2.14}$$

subject to the constraint $\|\mathbf{w}\|^2 = 1$, which results in [31] $\mathbf{w}^{ideal} = \frac{\mathbf{h}^*}{\|\mathbf{h}\|}$.

2.2.5 Co-Phase Feedback

The Ideal Feedback requires phase and amplitude information of the beamforming vector. A Co-phase Feedback scheme corrects the phases of the signals received from

different channels and adds them coherently, without using the amplitude information of the channel. The Co-phase Feedback algorithm may be shown as follows: $w^{(1)} = \frac{1}{\sqrt{M}}$, and $w^{(m)} = \frac{1}{\sqrt{M}}\, e^{-j(\phi^{(m)}-\phi^{(1)})}$ for $m = 2, \cdots, M$.

It has been shown that Ideal Feedback and Co-phase Feedback schemes enhance the (average) received SNR by a factor of M and $1 + (M-1)\frac{\pi}{4}$, respectively, with respect to the transmit SNR ($\text{SNR}_{tx} = \frac{E_s}{N_0}$) [24, 31]. This SNR gain is used as a figure of merit in an uncoded system. For $M = 2$, the SNR gains are 3.0 dB and 2.5 dB, respectively. Therefore, by using the phase-only information, we are losing only 0.5 dB of SNR (and at maximum 1.0 dB for large number of transmit antennas). This confirms that the channel phase information is usually more important than the amplitude information.

2.2.6 Quantized Co-phase Feedback

In practice, a limited capacity is available in the feedback channel. Therefore, for the quantization of the CSI, an efficient source-coding scheme is used. There are a variety of works on the quantization of feedback data, e.g. [32, 28, 33, 34, 35]. In this work, we focus on the closed-loop systems with the (quantized) co-phase feedback. It is assumed that $M = 2$, hence $\mathbf{h}_n = [h_n^{(1)}, h_n^{(2)}]$ and $\mathbf{w}_n = [w_n^{(1)}, w_n^{(2)}]$, where n is the time index. It is also assumed that the first beamforming weight is constant, i.e., $w_n^{(1)} = \frac{1}{\sqrt{2}}$, and $w_n^{(2)}$ is constructed from the feedback data.

Figure 2.2 shows the block diagram of a quantized co-phase[2] feedback system. In the figure, $\phi_n = \angle h_n^{(2)} - \angle h_n^{(1)}$ is the co-phase information, $\tilde{\phi}_n$ is the quantized co-phase, and I_n is the respective index. I_n is sent through the feedback channel

[2]The term co-phase refers to the phase difference between the two channels.

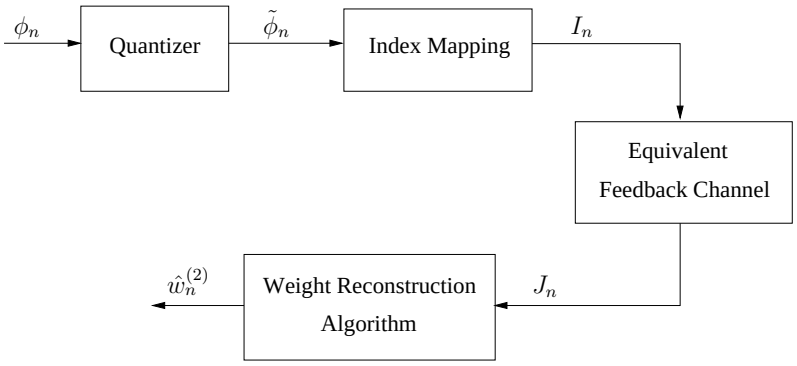

Figure 2.2: Block diagram of a quantized co-phase feedback system

and J_n is received at the base station, possibly delayed and/or noisy (I_n and J_n are also called feedback symbols in the sequel). J_n could be a hard-decided symbol or a soft-output of the channel. For an error-free feedback channel, $J_n = I_n$. Here, a memoryless feedback channel is assumed which makes our analysis easier. This assumption is valid in practice as the feedback has a low symbol rate.

At the transmitter, the phase information is used to calculate the beamforming weights, whereas the transmit power is constant. Hence, it is assumed $w_n^{(1)} = \frac{1}{\sqrt{2}}$ and $\left|w_n^{(2)}\right| = \frac{1}{\sqrt{2}}$. In an ideal co-phase feedback system, $\angle w_n^{(2)} = -\phi_n$.

2.3 Closed-Loop Mode 1 of 3GPP

The 3GPP standard has a closed-loop mode, called mode 1, which is adopted from the co-phase feedback scheme. Mode 1 is initially designed to provide service for low to moderate mobile speeds [36]. Whereas its performance degrades at higher mobile speeds. Improving the performance at higher mobile speeds is of great importance as it helps to accommodate a larger number of mobile users. This is one of the objectives of this chapter (and the next chapter) which is achieved by using the feedback data

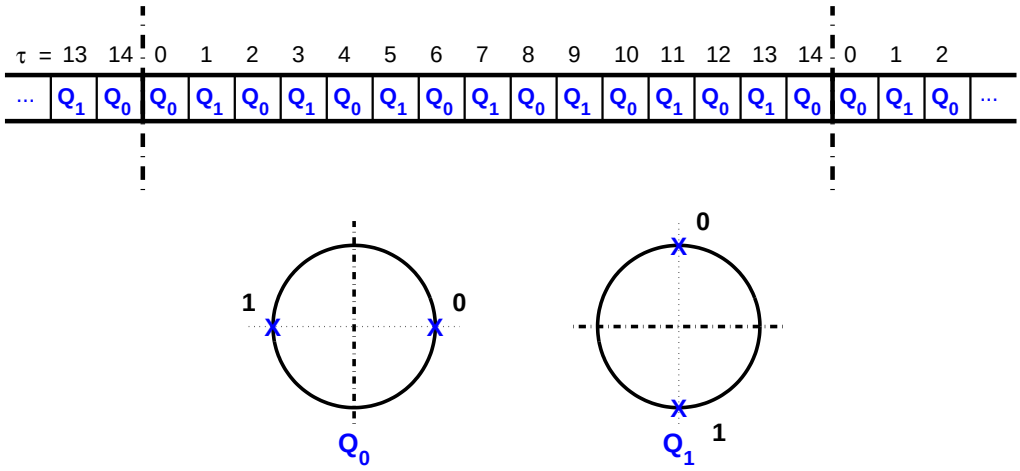

Figure 2.3: The framing structure and the quantizers of mode 1 of 3GPP

more efficiently in reconstructing the underlying beamforming vector. A detailed description of mode 1 comes next.

The closed-loop mode 1 of the 3GPP standard [1] is an example of the model introduced in Section 2.2.6. In mode 1, the quantization of the phase ϕ_n is subject to a special framing structure as shown in Fig. 2.3. Each (uplink) frame has a duration of 10 msec and includes 15 slots. Each slot contains a number of data symbols depending on the data rate. For each slot, one bit of feedback data is sent from the mobile unit which results in a feedback stream of 1500 bits per second. The feedback bit is determined by one of the two one-bit quantizers Q_0 and Q_1, according to Fig. 2.3, where $Q_0 = \{0, \pi\}$ and $Q_1 = \{\pi/2, -\pi/2\}$. Showing the relative place of each slot in a frame, we use a framed time index, $\tau = n \bmod 15$, hence in a frame, $\tau = 0, 1, \cdots, 14$.

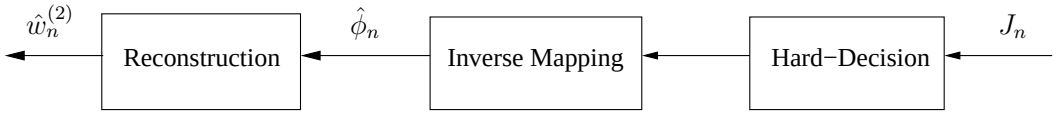

Figure 2.4: Block diagram of the weight reconstruction for mode 1 of 3GPP

2.3.1 Weight Reconstruction Algorithm

At the base station, after a hard-decision unit, the received feedback data bits are mapped to $\hat{\phi}_n$ phase stream according to Fig. 2.3, i.e., $\hat{\phi}_n \in Q_{\tau \bmod 2}$. The weight $w_n^{(2)}$ is constructed from the two recent phases, one from a Q_0 slot and one from a Q_1 slot. The reconstruction scheme can be shown as

$$\hat{w}_n^{(2)} = \begin{cases} \frac{1}{2}(e^{j\hat{\phi}_n} + e^{j\hat{\phi}_{n-1}}), & \tau \neq 0 \\ \frac{1}{2}(e^{j\hat{\phi}_n} + e^{j\hat{\phi}_{n-2}}), & \tau = 0. \end{cases} \tag{2.15}$$

Note that at each time, equation (2.15) selects the $\hat{w}_n^{(2)}$ from a set of 4 predefined weights. This construction also guarantees that $\left|\hat{w}_n^{(2)}\right| = \frac{1}{\sqrt{2}}$ for all n.

It is observed from Fig. 2.3 that $\tilde{\phi}_n$ (and similarly $\hat{\phi}_n$) can attain one of four values, $\tilde{\phi}_n \in \{-\pi/2, 0, \pi/2, \pi\}$. Therefore, index I_n could be defined as $I_n \in \{0, 1, 2, 3\}$, respectively. It is notable that these 2-bit symbols are constructed from the 1-bit feedback and the time information τ. Furthermore, equation (2.15) shows that the weight reconstruction block of mode 1 can be depicted as shown in Fig. 2.4. It is observed that the weight reconstruction algorithm has been separated into different parts in the standard, and can be potentially improved through a joint design, i.e., calculation of $\hat{w}_n^{(2)}$ directly from the sequence of J_n.

2.4 Effect of Feedback Error

One of the major problems associated with the downlink beamforming is the presence of errors in the (uncoded) feedback stream. If a feedback command for the base station becomes corrupted during the transmission in the uplink slot, an incorrect antenna weight vector will be applied at the transmitter. There are two consequences for such an error as follows.

First, the received signal power is smaller [23] because a non-optimum weight is applied. However, simulations show that the performance degradation due to this effect is rather small. The second consequence is much more serious. Assume that $\hat{\mathbf{w}}$ is applied at the transmitter. Similar to (2.12), we have

$$z = v^H \mathbf{h}^T \hat{\mathbf{w}} s + v^H \eta \tag{2.16}$$

where z is the decoding metric. Hence, the receiver should be able to calculate $\mathbf{h}^T \hat{\mathbf{w}}$ (called dedicated channel estimate [37]) for calculation of the optimum v. The mobile unit obtains the dedicated channel estimate by combining the estimates for the individual antennas from the common pilots with the assumed weight vector $\mathbf{w}$. However, each time a feedback error occurs, $\mathbf{w}$ at the mobile unit is different from the actual $\hat{\mathbf{w}}$ that is applied at the base station, because the mobile unit is unaware of the error occurrence in the feedback channel. Each of these mismatches in the dedicated channel estimate can potentially result in an error in the decoding process. Therefore, an error floor proportional to the feedback error is imposed on the performance.

The loss of the closed-loop gain because of the feedback error (the first effect) has been analyzed in [23]. To minimize the effect of the mismatch problem (the second effect), a technique called Antenna weight Verification (AV) [37] has been suggested.

The AV technique is explained in the next section.

2.4.1 Antenna Weight Verification

In an Ideal AV, the mobile unit always knows the exact weight $\hat{\mathbf{w}}$ applied at the base station. Ideal AV theoretically eliminates the mismatch effect, but it is practically impossible to implement when the feedback information is corrupted. In a practical AV algorithm, the mobile station considers the possibility of an erroneous feedback transmission. This is done by a hypothetical comparison between the common-pilot-based channel estimate and the one obtained from a few training symbols in the dedicated channel which include the effect of $\hat{\mathbf{w}}$. An AV algorithm for mode 1 of 3GPP has been suggested in the annex to [1], and the performance of the AV algorithm has been analyzed in [38]. A trellis-based AV algorithm has been proposed in [13] to improve the performance of the verification process.

However, the AV technique has some drawbacks. Applying an AV algorithm requires extra calculations at the mobile unit, and also requires special dedicated preamble bits to be transmitted to all the users. Also, the structure of an AV algorithm is based on the beamforming scheme applied at the transmitter, which means that the AV algorithm is different for each beamforming algorithm. Furthermore, AV can not decrease the loss of the closed-loop gain (first effect), as it is implemented at the mobile unit. Due to these problems, there is a tendency to find an alternative technique for AV (for example see [39]).

In the next section, we introduce a new approach to improve the performance of the beamforming scheme, especially in the presence of feedback error. In this approach, the redundancies available in the feedback data are exploited to find an

improved estimate of the antenna weight, without the need for any preamble data sequence. Our approach helps solving both of the aforementioned problems, as it provides a better reconstruction scheme for the weights. It decreases the effect of the feedback error which reduces the mismatch effect. It is notable that our algorithms can be used along with an AV algorithm. However, the performance results show the possibility of using our algorithms without the need for an AV algorithm in some cases. Comparison between the conventional method in conjunction with the Ideal AV and one of our algorithms show that at low to moderate mobile speeds, our algorithm achieves the same performance without using AV.

2.5 Efficient Reconstruction of the Beamforming Weight

In the sequel, a feedback link consistent with Fig. 2.2, and defined in Section 2.2.6 is assumed. The framing structure and the quantization scheme of mode 1 of the 3GPP standard, described in Section 2.3, is preserved here. However, more efficient reconstruction algorithms are presented. Unlike the method suggested in the standard, effect of feedback error is considered in the reconstruction algorithms. Feedback delay is not considered here and is the subject of the next chapter. The next section elaborates on an MMSE criteria for the reconstruction which results in a number of proposed algorithms. Also, using a MAP (Maximum A Posteriori) criteria, other algorithms are presented.

μ	1	2	3	4
4^μ	4	16	64	256
Codebook Size	4	12	32	80

Table 2.1: Codebook size

2.5.1 MMSE Approach

The fundamental theorem of estimation states that given the received sequence $\underline{J}_n = [J_1, J_2, \cdots, J_{n-1}, J_n]$, the Minimum Mean-Squared Error (MMSE) estimate of the weight is $\hat{w}_n^{(2)} = E\left[w_n^{(2)} | \underline{J}_n\right]$. It has been shown [40, 41] that the above formula can be approximated by the following expression:

$$\hat{w}_n^{(2)} \cong \sum E\left[w_n^{(2)} | \underline{I}_n^{n-\mu+1}\right] P\left(\underline{I}_n^{n-\mu+1} \,|\, \underline{J}_n\right), \tag{2.17}$$

where the summation is over all the possible μ-fold sequences of $\underline{I}_n^{n-\mu+1}$, where $\underline{I}_n^{n-\mu+1} = [I_{n-\mu+1}, \cdots, I_{n-1}, I_n]$. In the MMSE sense, the formula is asymptotically optimum for sufficiently large values of μ [40].

In equation (2.17), $E\left[w_n^{(2)} | \underline{I}_n^{n-\mu+1}\right]$ is a non-linear estimator for the weight. In fact it defines a *codebook* as

$$w_{CB}(\underline{i}_n^{n-\mu+1}) = E\left[w_n^{(2)} | \underline{I}_n^{n-\mu+1} = \underline{i}_n^{n-\mu+1}\right], \tag{2.18}$$

where $\underline{i}_n$ is a possible realization of $\underline{I}_n$. It is shown in Appendix A that the codebook has $(\mu + 1)\, 2^\mu$ codewords, which is less than 4^μ possible codewords. This is because there are some constraints on the value of i_n imposed by the framing structure discussed earlier. Table 2.1 shows the codebook size for some typical values of μ.

γ (Markov order)	0	1	2	3	4
$V = 1$ kmph	0.01	0.78	1.61	1.67	1.69
$V = 5$ kmph	0.01	0.78	1.48	1.53	1.55
$V = 25$ kmph	0.01	0.76	1.12	1.14	1.16
$V = 100$ kmph	0.01	0.73	0.75	0.76	0.78

Table 2.2: Redundancies $R(\gamma)$ for different memory depths γ, and different mobile speeds

2.5.2 Trellis Structure

For capturing the redundancies in the feedback bitstream, we assume that the bitstream follows a Markov model of order γ. A trellis structure is set up based on the Markov model to exploit the redundancies. The states of the trellis are defined as $S_n = \underline{I}_n^{n-\gamma+1}$. There are totally $(\gamma + 1)\, 2^\gamma$ possible states (See Appendix A). Given a value for γ, The trellis is specified by the probabilities of the state transitions, $P(S_n|S_{n-1})$, or equivalently, by the conditional probabilities $P(I_n|S_{n-1})$. These are the A Priori Probabilities (APP) of the Markov model, and can be calculated and stored as a lookup table.

To find a proper value for γ, we examine the redundancies defined as $R(\gamma) = 2 - H(I_n|S_{n-1})$, where $H(I_n|S_{n-1})$ is the average conditional entropy. Table 2.2 shows typical redundancies for values of $\gamma = 0, 1, 2, 3, 4$, at different mobile speeds in the range of our interest. As expected, it is observed that redundancies are higher for larger values of γ. However, for $\gamma \geq 2$, redundancies do not increase significantly, which means there is no significant residual redundancy [42] left in the sequence after that depth. Hence, we use $\gamma = 3$ in our simulations which is a small value, yet captures most of the redundancies. The resulting trellis, which has 32 states, is used in some of our algorithms.

To implement (2.17), a proper value of μ is also required. Considering (2.18), the value of μ should be chosen to include the number of feedback symbols that carry some useful information about the codeword. The redundancies are limited to a certain depth, beyond which a larger μ does not improve the performance. With experiment, the value is chosen as $\mu = 3$.

2.5.3 Time-Dependency of the Trellis

As discussed in Section 2.3, the quantization process is subject to the framing structure of mode 1 which is *time-dependent*. In each slot, I_n can adopt one of the four values $\{0, 1, 2, 3\}$, which represents a 2-bit value. One of these bits is the information bit which is transmitted via feedback channel, and the other bit is specified by the slot number. In other words, given the time slot, I_n attains one of two possible values. Therefore, the trellis structure is periodically time-dependent. Fig. 2.5 shows all possible paths on a typical trellis for $\gamma = 2$.

As discussed in Appendix A, there are total $(\gamma + 1)2^{\gamma}$ possible states. However, some states occur only at the frame-boundary, whereas the others can occur within a frame. In other words, in each time slot specified by τ, some states never happen. For 2^{γ} states (corresponding to $n_{win} = 0, 2, 4, \cdots, 12$, in Fig. 2.6), the next symbol could be any of the four possible values because those states can occur both in the middle of a frame and at the boundary. Assuming that the slot number is known, these states can be split into two categories subject to the different framing effects. Hence, given the slot number τ, each state is connected to only two states, as can be observed in Fig. 2.5. Therefore, it is appropriate to use $P(S_n|S_{n-1}, \tau)$ instead of $P(S_n|S_{n-1})$ to capture the time-dependency of the trellis. Because there are less possible paths on

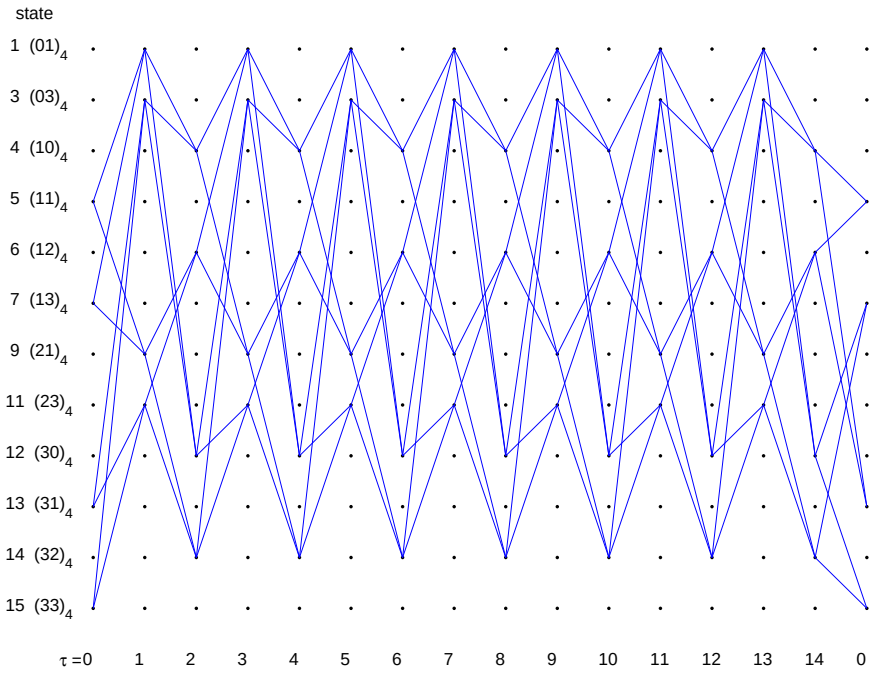

Figure 2.5: Time-based trellis for the case $\gamma = 2$

the trellis, the time-based approach can decrease the complexity of the trellis by a factor of $2(\gamma + 1)$.

2.5.4 Normalized-MMSE Algorithm (NMMSE)

We are dealing with the estimation of a complex variable with a constant amplitude, as $\left|\hat{w}_n^{(2)}\right| = \frac{1}{\sqrt{2}}$. However, there is no control on the amplitude of the MMSE estimate $\hat{w}_n^{(2)}$ provided by (2.17). Hence, we need an MMSE estimator with a constant amplitude constraint, which is introduced in Lemma 1, next.

Lemma 1. *Consider the random variable w with $|w| = \beta$. Assume that $\hat{w}^{normal}$ is the constant-amplitude MMSE estimation of w. Given $\left|\hat{w}^{normal}\right| = \alpha$, then*

$$\hat{w}^{normal} = \alpha \frac{E[w]}{|E[w]|}. \tag{2.19}$$

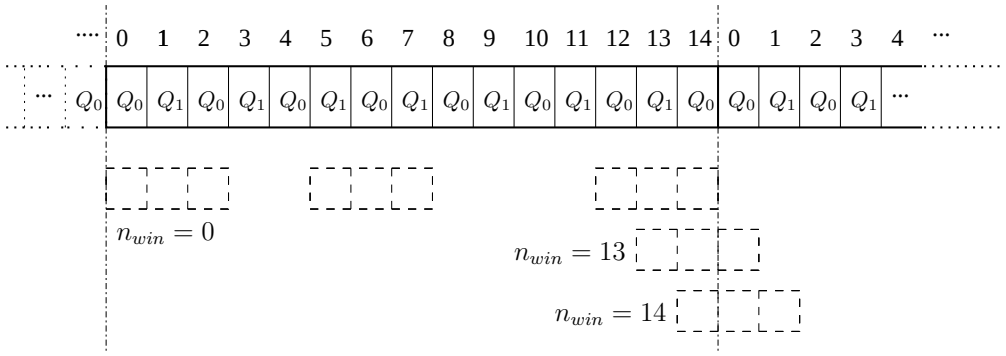

Figure 2.6: Calculation of the number of states

Proof. See Appendix B. □

According to Lemma 1, we can always calculate the needed antenna weight using the MMSE solution of (2.17) as

$$\hat{w}_n^{(2)\,normal} = \frac{1}{\sqrt{2}} \frac{\hat{w}_n^{(2)}}{\left|\hat{w}_n^{(2)}\right|}. \tag{2.20}$$

Implementing (2.17), the probabilities of the possible states of the trellis are required at each time. We have assumed a Markov model and a memoryless feedback channel, so using the BCJR algorithm [43] the states probabilities can be computed recursively by [40]

$$\begin{aligned} P(S_n|\underline{J}_n) &= C \cdot P(J_n|I_n) \cdot \\ &\sum_{S_{n-1} \to S_n} P(I_n|S_{n-1}) P(S_{n-1}|\underline{J}_{n-1}) \end{aligned} \tag{2.21}$$

where the summation is over all the possible transitions from the states at time $n-1$ to S_n, and C is the normalizing factor such that $\sum_{S_n} P(S_n|\underline{J}_n) = 1$. $P(I_n|S_{n-1})$'s are available as APP, and $P(J_n|I_n)$'s are the channel transition probabilities. Assuming a Binary Symmetric Channel (BSC) with the error probability of p_e for transmitted feedback bits, the equivalent feedback channel (Fig. 2.2) is represented by $P(J_n|I_n)$,

where $P(I_n|I_n) = 1 - p_e$, $P(J_n|I_n) = p_e$ if $J_n \neq I_n$ but both belong to the same quantization set, otherwise $P(J_n|I_n) = 0$.

For simplicity, we assume that $\mu \leq \gamma$. Then the required probabilities in (2.17) are directly calculated using (2.21), as

$$P\left(\underline{I}_n^{n-\mu+1} \,|\, \underline{J}_n\right) = \sum P(S_n|\underline{J}_n), \tag{2.22}$$

where summation is over all the states S_n that include the $\underline{I}_n^{n-\mu+1}$ sequence. This assumption eliminates the need for the backward recursion of the BCJR algorithm.

2.5.5 Non-Linearly-Estimated Weight Algorithm (NLW)

Simplifying the MMSE algorithm, assume that the feedback stream is error-free. In this case, equation (2.17) reduces to a codeword selection, and lemma 1 is used to guarantee the weight normalization. Because the codeword is a non-linear estimator of the weight in comparison with the linear codewords of the standard, we call the algorithm the NLW algorithm.

In NLW algorithm, the received feedback sequence is taken as the estimate of the transmitted sequence, $\hat{i}_n = j_n$, where j_n is the hard-decided received feedback symbol, and it is used to generate the index for the codeword, i.e.,

$$\hat{w}_n^{(2)} = w_{CB}\left(\hat{\underline{i}}_n^{n-\mu+1}\right), \tag{2.23}$$

which is applied to (2.20). NLW algorithm is generally suboptimum, however it is asymptotically optimum for the error-free feedback case.

2.5.6 Sequence MAP Algorithm (SMAP)

The Sequence MAP decoder [40, 44] receives the sequence $\underline{J}_n$ and determines the most probable transmitted sequence as $\hat{\underline{i}}_n = \arg\max P(\underline{I}_n|\underline{J}_n)$, using the trellis of Section 2.5.2. Considering the memoryless property of the feedback channel, the following branch metric can be obtained for the respective trellis [40],

$$m\left(J_n, S_{n-1} \xrightarrow{I_n} S_n\right) = \log\left\{P(J_n|I_n)\, P(I_n|S_{n-1})\right\}, \tag{2.24}$$

which is used within the well-known Viterbi algorithm to find the solution. The estimated sequence is applied to (2.23), then the beamforming weight is calculated by (2.20). Note that SMAP algorithm could be used to exploit the trellis with a lower computational complexity in comparison with the MMSE solution.

2.5.7 Soft-Output Methods (Soft-SMAP and Soft-NMMSE)

The use of soft feedback data [45] can potentially improve the performance of the SMAP and NMMSE algorithms. In the soft methods, it is assumed that instead of hard-decided bits of feedback data, soft-output (noisy) symbols are available. In other words, instead of a BSC feedback channel, an AWGN channel with binary input is assumed. The noise power is selected to keep the hard-decision feedback error probability the same for the two cases.

2.5.8 Implementation and Complexity

Note that the algorithms which have been proposed here are real-time, and decide on the needed antenna weight without any delay. Receiving the most recent feedback symbol J_n, each algorithm calculates $\hat{w}_n^{(2)}$ to be applied at the transmitter. At the

receiver, the transmitted feedback sequence $\underline{I}_n = \underline{i}_n$ is available. Hence, to calculate the combining variable v_n, the receiver calculates its estimate of the weights using the codebooks, as in the error-free case. In other words, the base station uses one of the proposed algorithms to calculate the weights, while the mobile unit just needs to select the $\underline{i}_n^{n-\mu+1}$-th weight out of a normalized codebook (similar to the NLW algorithm).

The codebook and APP are calculated off-line. The calculation process of the codebooks for different channel models is the same, as explained in Section III-A. We use Jakes fading model, and these codebooks are calculated once for each mobile speed corresponding to different doppler frequencies, using sufficient amount of training data. For selecting the proper codebook, an estimate of the mobile speed is required. There are various algorithms suggested for a general mobile speed estimation [46] or in particular for 3G systems [47, 48]. It is shown in the simulation results that for the estimation accuracies reported in the above references, the performance of our algorithms do not change significantly. In other words, the proposed algorithms are robust to the mobile speed estimation error. Therefore, a small number of codebooks, corresponding to a small number of mobile speeds, are sufficient to cover the entire range.

Regarding the computational complexity, our algorithms use known methods like Viterbi algorithm and forward recursion of the BCJR algorithm with small memory depths. Therefore, the complexity is relatively low. Furthermore, these algorithms are implemented at the base station where complexity is not of great concern. Even though, using the time-dependency of the trellis, the complexity of our trellis-based algorithms could be further decreased. Table 2.3 shows the requirements of each of

Our Algorithm:	NLW Algorithm	SMAP, Soft-SMAP	NMMSE, Soft-NMMSE
codebook	Yes	Yes	Yes
APP		Yes	Yes
Trellis Processing		Viterbi	Forward-BCJR

Table 2.3: Implementation requirements of our algorithms at the base station

our algorithms at the base station. At the mobile unit, only codebooks are required, as the NLW algorithm is implemented regardless of the specific algorithm used at the base station.

2.6 Numerical Results

2.6.1 Simulation Parameters

For the testing and comparison of the algorithms, we have simulated a communication system similar to the downlink of FDD WCDMA [5]. Fig. 2.7 represents our complete system, including the channel coding and the details of the feedback system. As channel code, Turbo coding [49] is used which parameters are suggested by the 3GPP standard [50] as shown in Table 2.4. In CDMA systems including WCDMA, there is a power control scheme intended to eliminate the slow fading. Therefore, we assume that slow fading is compensated by power control. Table 2.5 is a summary of the parameters of our simulations. Also it is assumed (only in this chapter) that the channel estimation is ideal. The other parameters, that may change in different simulations, are specified in each case. Also no antenna verification is used with the closed-loop algorithms, unless stated otherwise.

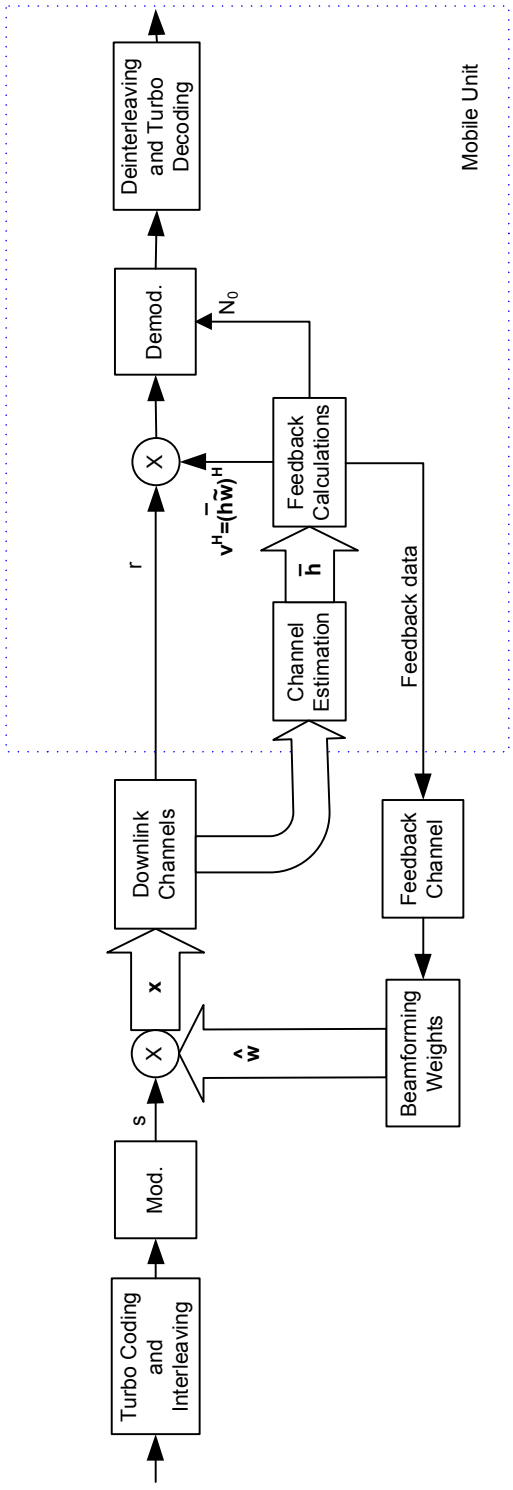

Figure 2.7: Block diagram of our feedback system

Coding Rate	1/3
No. of Memory Elements	3
Constituent Encoders (Convolutional)	$G_{bwd} = 1 + D^2 + D^3$ $G_{fwd} = 1 + D + D^3$
Output Pattern (P/S)	$\cdots, X_k, Z_k, Z'_k, \cdots$

Table 2.4: Turbo code parameters

Carrier Frequency	2.15 GHz
Modulation	QPSK
Transmitter	2 Antennas
Receiver	1 Antenna
Data Rate	15000 bps
Feedback Rate	1500 bps
Channel Model	Modified Jakes
Channel Coding	Turbo Code
Code Rate	1/3
Frame Length	300 (20 msec)
Bit Interleaving	One Frame
Power Control	Not applied

Table 2.5: Simulation parameters

2.6.2 Simulation Results

As a measure of performance, we use Frame Error Rate (FER), which is appropriate for a coded communication system. The overall performance of the system is determined by the interplay of feedback error rate, and mobile speed. Feedback error degrades the beamforming performance, and can result in an error floor effect as mentioned before. On the other hand, increasing the mobile speed improves the decoding performance in the forward link (as a result of increasing the fading diversity [26]), but generally degrades the performance of the feedback reconstruction algorithms to different extents. Therefore, given a feedback error rate, algorithms perform variously over different mobile speeds.

The following algorithms have been considered in the simulations: Standard (closed-loop mode 1 of 3GPP), NLW, SMAP, Soft-SMAP, NMMSE, and Soft-NMMSE, which are in the ascending order of complexity. It is assumed that $\gamma = 3$ and $\mu = 3$. Figs. 2.8 and 2.9 show the FER performance of the algorithms versus transmit SNR for 5% feedback error, and for the mobile speeds of $V = 1, 5, 25$ and 100 kmph. Figs. 2.10 and 2.11 similarly show the FER in 10% feedback error.

It is observed from Figs. 2.8-2.11 that our algorithms outperform the standard and result in significant savings in the transmit power. Regarding the relative gain of the algorithms, Figs. 2.12 and 2.13 show the required-SNR for a fixed FER versus the mobile speed, in 5% and 10% of feedback error, respectively. The plots include the standard algorithm with an Ideal AV, explained in Section 2.4.1. The performance of standard-IAV is the best performance which is achievable by using an AV algorithm along with the standard algorithm, hence it is a performance bound on using an AV algorithm. It is observed that NMMSE and Soft-NMMSE perform similar or even

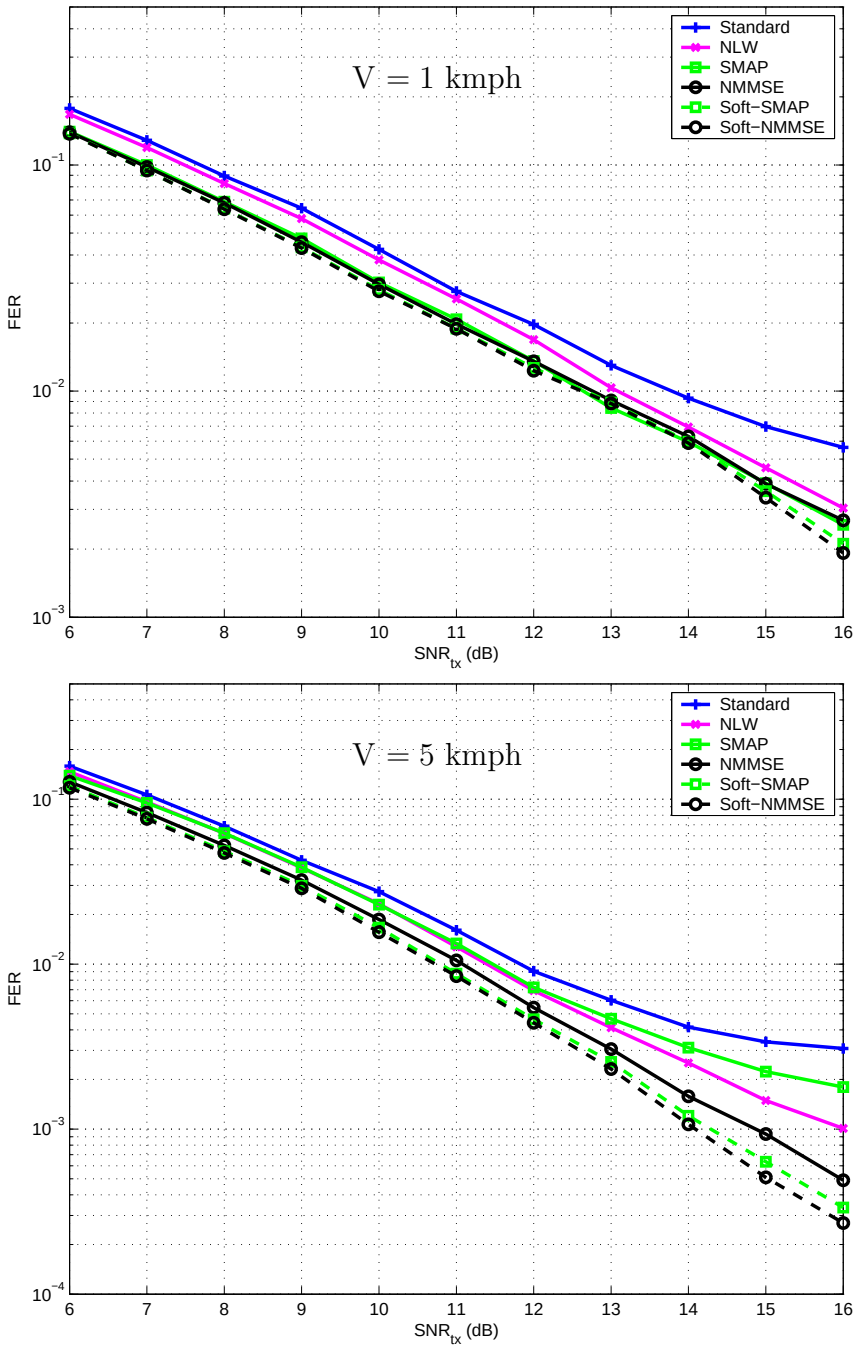

Figure 2.8: FER versus transmit SNR in 5% feedback error for V = 1 and 5 kmph

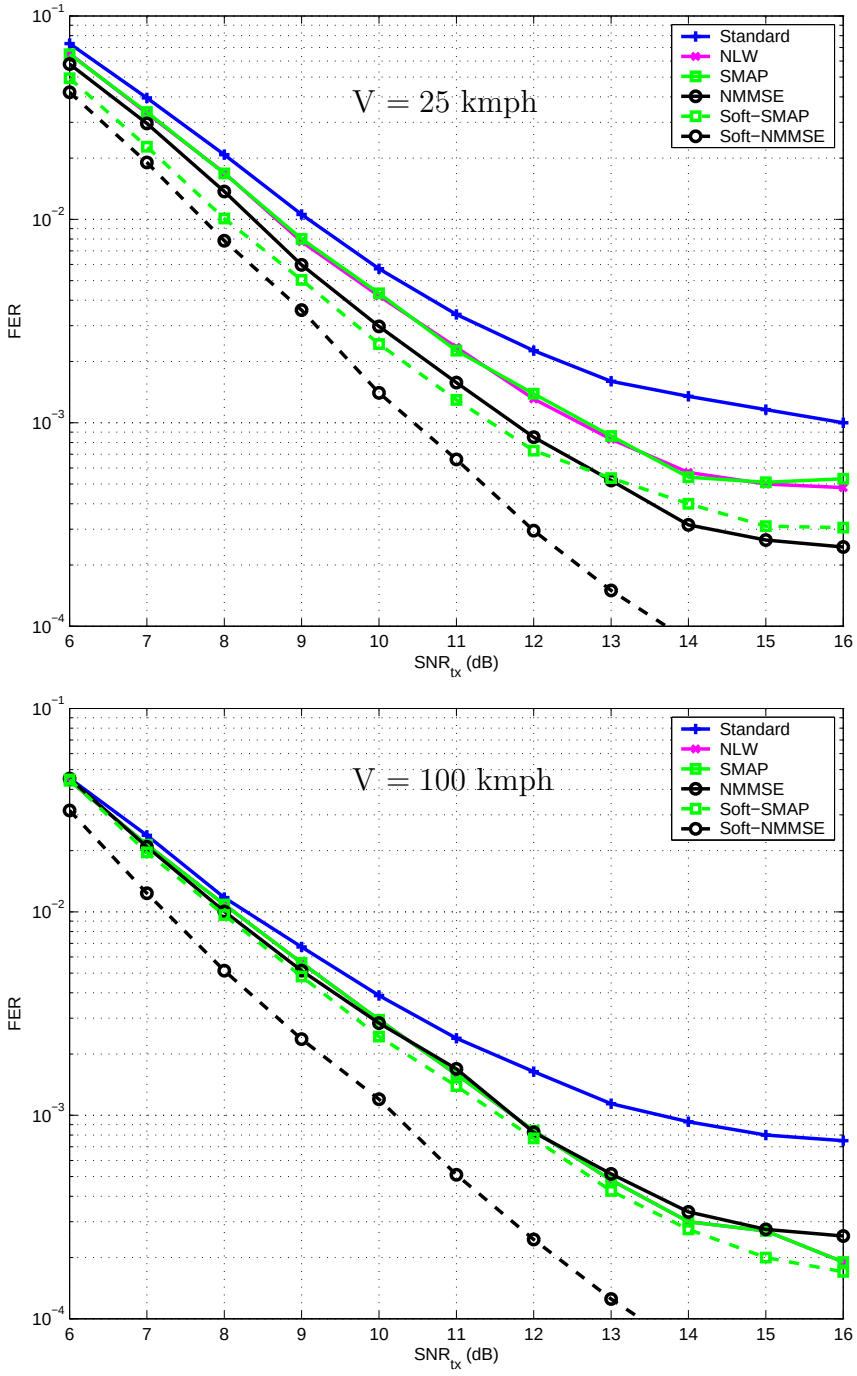

Figure 2.9: FER versus transmit SNR in 5% feedback error for V = 25 and 100 kmph

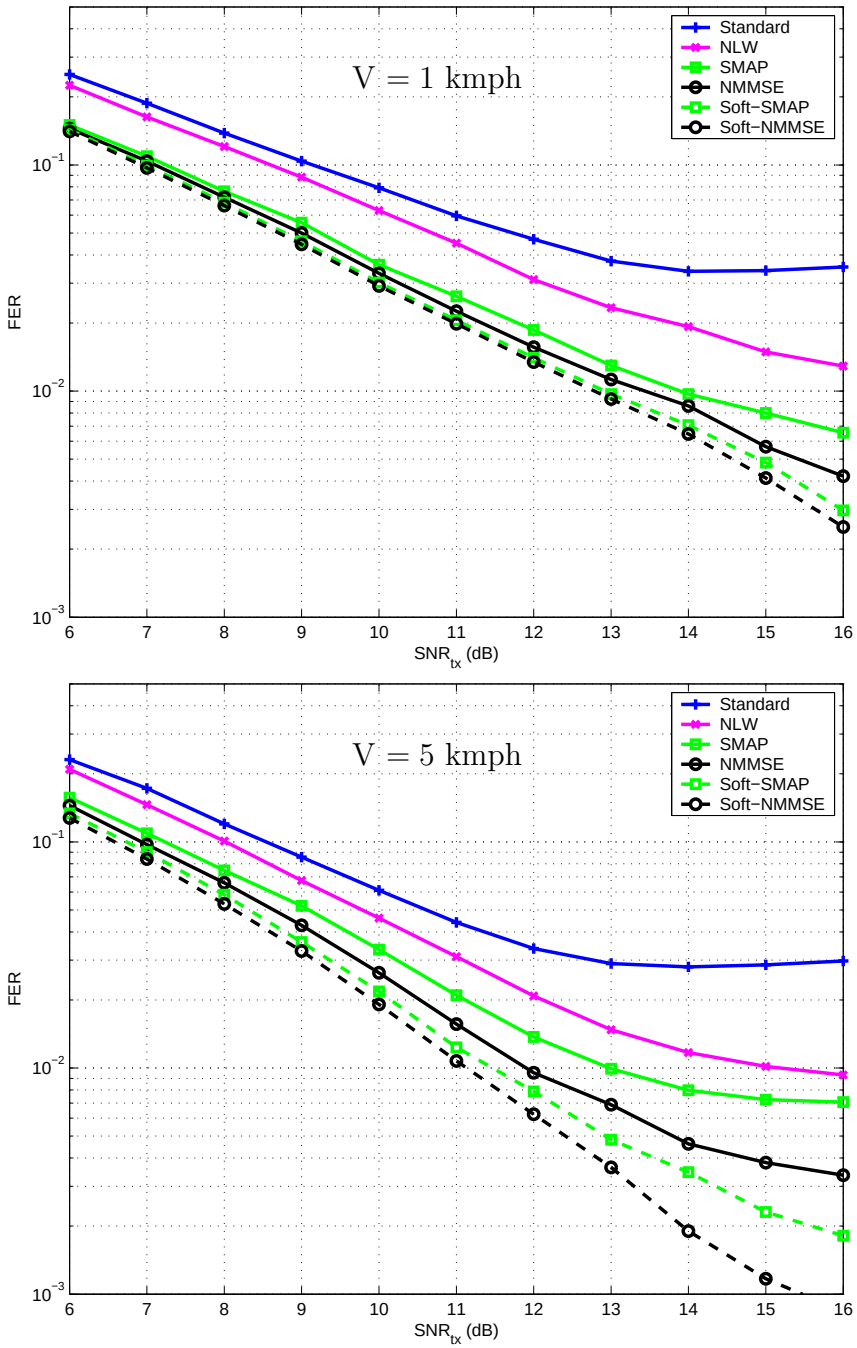

Figure 2.10: FER versus transmit SNR in 10% feedback error for V = 1 and 5 kmph

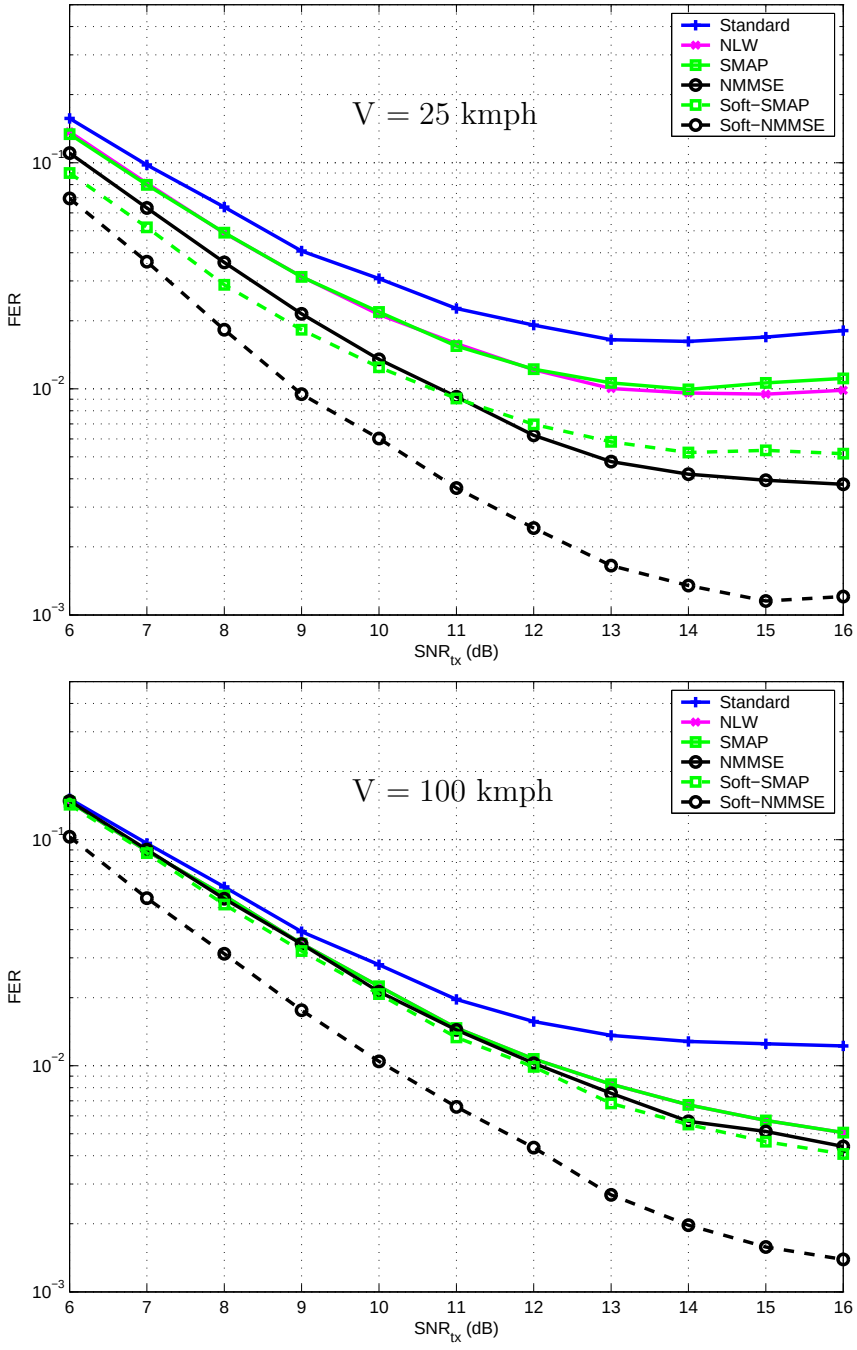

Figure 2.11: FER versus transmit SNR in 10% feedback error for V = 25 and 100 kmph

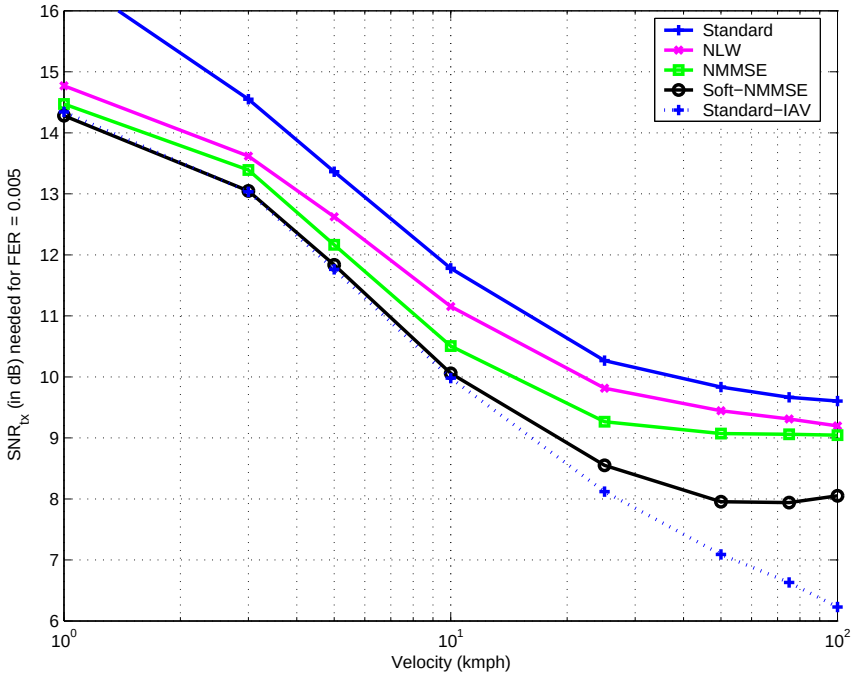

Figure 2.12: Required SNR versus mobile speed for FER=5e-3 in 5% feedback error

better than the standard-IAV bound for low to moderate mobile speeds. Fig. 2.12 shows that our approach can decrease the transmit power by more than 2 dB for low to high mobile speeds. This gain is higher for a smaller target FER or for a higher feedback error rate.

Regarding the effect of mobile speed and feedback error rate on the performance, following observations can be made from Figs. 2.8 - 2.13: At low mobile speeds, the reconstruction algorithms perform in this ascending order: first Standard, then NLW, and then the rest of the algorithms (which utilize APP) perform similarly, in particular at low SNR's. With increasing speed, the performance of the algorithms starts to differ. Soft-NMMSE and NMMSE algorithms outperform their SMAP counterparts. As expected, utilizing soft output improves the performance of the corresponding

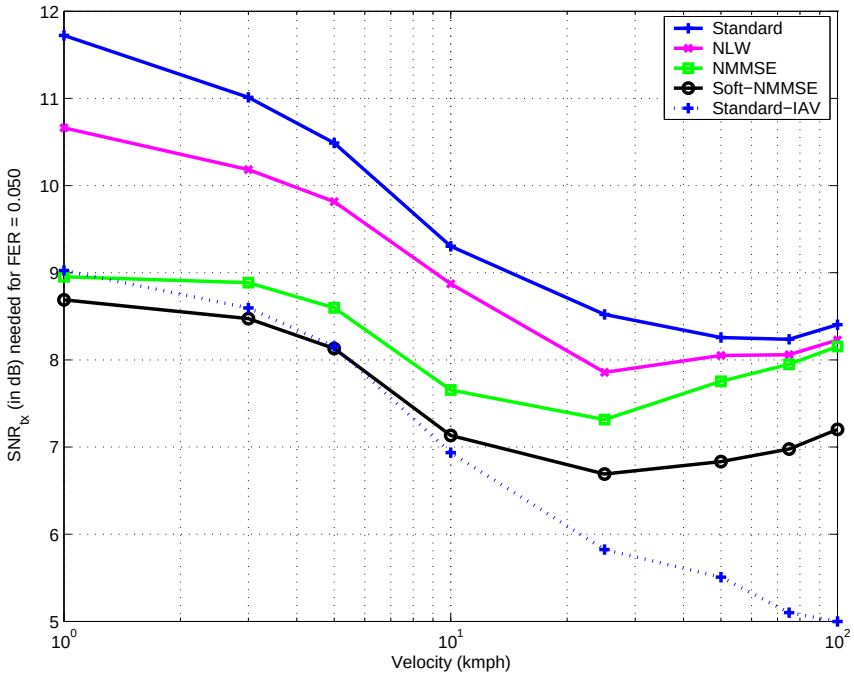

Figure 2.13: Required SNR versus mobile speed for FER=5e-2 in 10% feedback error

algorithms. At high mobile speeds, the channel changes rapidly, and the redundancy in the feedback bit stream diminishes. Therefore, the SMAP approach reduces to Maximum Likelihood detection (see Equation (2.24)), and Soft-SMAP performs like SMAP (This phenomenon is similarly observed from Fig. 9 in [40]). However, the Soft-NMMSE algorithm still utilizes the soft-outputs efficiently, and substantially outperforms the other algorithms. Note that in each algorithm, the effect of error floor on FER is higher for a larger feedback error rate, and at higher SNR's. The Soft-NMMSE algorithm provides the best performance at all mobile speeds and feedback error rates.

Actual Speed (kmph)	3	5	10	25	50	75	100
Lower Estimate	1	1	5	15	40	60	80
Higher Estimate	5	10	15	30	60	90	125

Table 2.6: Actual, lower and higher estimates of the mobile speed

2.6.3 Sensitivity to the Speed Estimation Error

As explained before, codebook and APP are chosen using an estimate of the mobile speed. Hence, the effect of the estimation error on the performance is investigated. As an example, we consider the Soft-NMMSE algorithm, which has the best performance among our algorithms and uses both codebook and APP. At a given mobile speed, we apply the codebooks related to a higher and a lower mobile speed to the algorithm, as shown in Table 2.6. The estimation errors used in the table are higher than the ranges reported for speed estimation algorithms [46, 47, 48]. The results shown in Fig. 2.14 indicate that the algorithm is not sensitive to the mobile speed estimation error. Therefore, a limited number of codebooks can be used to cover the entire range of the mobile speeds.

2.7 Conclusion

The closed-loop transmit diversity, which uses a combination of transmit diversity and channel feedback, is recognized as a promising approach to achieve high data rates in mobile communications. In 3GPP systems, however, the performance of the closed-loop scheme is limited, which is the result of the rate limit and error in the feedback channel and also the non-optimum weight reconstruction algorithm suggested in the standard. In this chapter, we propose an approach to improve the performance of the closed-loop system in the presence of feedback error, without

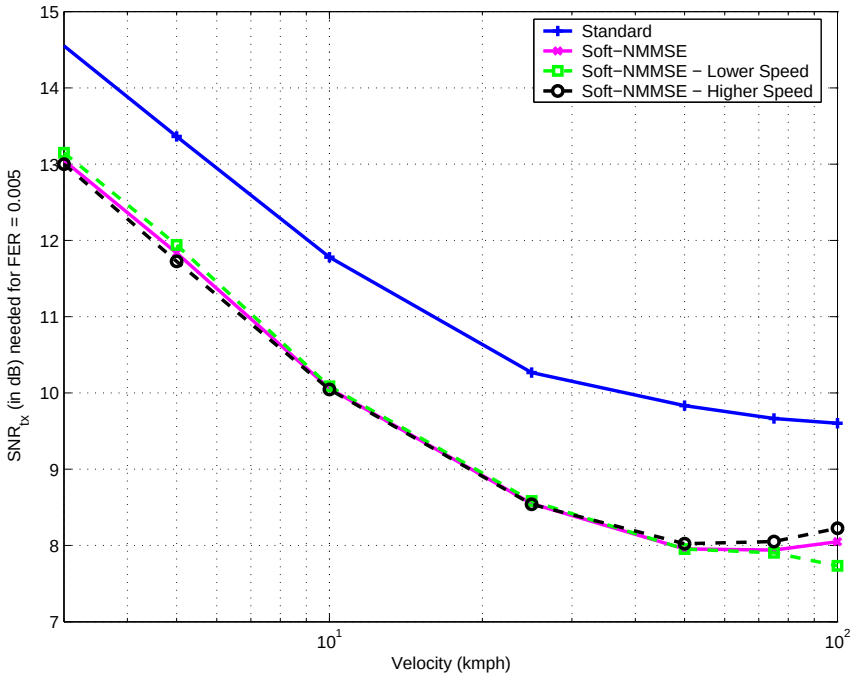

Figure 2.14: Required SNR versus mobile speed for FER=5e-3 in 5% feedback error: Sensitivity to the speed estimation error

changing the structure of the standard. We have introduced a number of algorithms to improve the performance of mode 1 of 3GPP. It has been shown that our algorithms can provide significant gains over the conventional approach at all mobile speeds. The performance of our algorithms, which do not need any preamble, are usually good enough such that an AV algorithm is no longer required. Though, an AV could be used along with our algorithms for further improvement. Moreover, our proposed algorithms are implemented mostly at the base station, as opposed to AV which increases the complexity of the mobile unit.

Chapter 3

Feedback Delay in Closed-loop Wireless Systems

The closed-loop transmit diversity technique is used to improve the performance of the downlink channel in MIMO communication systems. In these closed-loop systems, feedback delay and feedback error, as well as the sub-optimum reconstruction of the quantized feedback data, are the usual sources of deficiency. We address the efficient reconstruction of the beamforming weights in the presence of the feedback imperfections, by exploiting the residual redundancies in the feedback stream. Focusing on the issue of feedback delay, we propose two approaches to improve the performance. One is based on using a channel predictor at the receiver to compensate for the delay, and using a JSCC method (similar to the one introduced in the previous chapter) to compensate for the feedback error. Another approach deals with the feedback imperfections in a unified reconstruction algorithm using JSCC techniques. Furthermore, we introduce the concept of Blind Antenna Verification which can substitute the conventional Antenna Weight Verification process without the need for any training data. The closed-loop mode 1 of the 3GPP standard is used as a benchmark, and the performance is examined within a WCDMA simulation framework. It is

demonstrated that the proposed algorithms outperform the conventional methods at all mobile speeds, and are suitable for the implementation in practice.

3.1 Introduction

In a downlink closed-loop system, the transmitter receives the required CSI through a limited-capacity feedback channel from the receiver. The feedback data is a low-rate bitstream resulting from rough quantization of the CSI at the receiver. There are three major imperfections which affect the closed-loop systems: feedback delay, feedback error, and sub-optimal reconstruction. Feedback delay has been shown to drastically affect the performance of closed-loop systems [8, 9, 51, 24, 52], as the transmitter has to use outdated CSI. This problem gets worse as the mobile speed increases because the channel is changing more rapidly.

The feedback data is usually uncoded, or has a low-rate coding. Hence, a closed-loop scheme is sensitive to the errors in the feedback channel as explained in the previous chapter. Other than decreasing the closed-loop gain, feedback error causes another more serious problem. For decoding purposes, the receiver needs to know exactly what weights have been applied at the transmit antennas. However, the receiver is not normally aware of the location of the errors in the feedback channel, which causes mismatch at the receiver. This mismatch imposes an error floor on the system performance which is proportional to the feedback error rate as each feedback error can potentially result in symbol errors in the respective slot. In many research works, an impractical assumption is made that the receiver somehow knows the exact transmitter weights at all times. Ratifying this problem in practice, an *Antenna-weight Verification* algorithm, also called *Antenna Verification* algorithm (AV), [1] is

applied which needs some extra training data at the receiver for each user. There are a few works in the literature on the AV problem, such as [13, 53, 38]. These articles address the problem for the closed-loop modes of the 3GPP standard, when the dedicated training data is available. In this chapter, we are interested in the AV problem without using any extra training, i.e, in a blind fashion. A recent paper [54] deals with a similar problem, however, for a single transmit-antenna selection system. Optimizing the signaling assignment, it has been shown that verification of the selected antenna at the receiver is crucial when the feedback is erroneous. Furthermore, a number of blind and non-blind AV methods have been proposed for the antenna selection system [54].

The reconstruction schemes used in closed-loop systems are usually not optimal due to simplifications of the algorithms, and ignoring the feedback error and delay. Our focus here is on Mode 1 of 3GPP [1] (as described in Section 2.3) which only feeds back the phase information of the channel with a special quantization scheme. Despite all the imperfections, Mode 1 has a good performance at low mobile speeds, but it fails at higher speeds. In the previous chapter, the efficient reconstruction of beamforming weight in the presence of feedback error is addressed. Some JSCC techniques are used to improve the performance of Mode 1 of 3GPP, by taking advantage of the redundancy available in the CSI stream.

In this chapter, we consider the problem of feedback delay, as well as feedback error, in a closed-loop system. To solve this problem, we propose two approaches. One approach uses predicted channel values to compensate for the effect of feedback delay, and uses the JSCC method for the feedback error. In the other approach, a unified JSCC framework deals with the feedback imperfections. Exploiting the novel

concept of Blind Antenna Verification, this method only uses the feedback bitstream and does not need any type of training data. The performance of the algorithms is examined in the framework of the closed-loop mode 1 of the 3GPP standard. For the channel model, we consider spatially-uncorrelated Rayleigh fading channels. In the simulations, we use a separate Jakes fading generator introduced in [27] for each channel.

3.2 Efficient Reconstruction of the Beamforming Weight

In the sequel, we assume the framing structure and the quantization scheme of the closed-loop mode 1 of the 3GPP standard [1], as described in the previous section. However, our approach can be used for any other feedback scheme as well.

3.2.1 MMSE Solution in the presence of Feedback Delay and Error

In the previous chapter, the MMSE algorithm in the presence of noisy feedback is introduced. The best algorithm is obtained when soft-output is used (i.e., assuming that J_n is available before a hard-decision operation), and it is called *SoftNMMSE* (Soft-Normalized-MMSE). In the following, a similar approach is pursued when the feedback data is delayed as well.

Assuming a delay of d symbols in the feedback channel (d is a non-negative integer), the sequence $\underline{J}_{n-d}$ is available at the base station at time n. The fundamental

theorem of estimation states that given $\underline{J}_{n-d}$,

$$\hat{w}_n^{(2)} = E\left[w_n^{(2)} \middle| \underline{J}_{n-d}\right] \tag{3.1}$$

is the minimum mean-squared error (MMSE) estimate of the weight $w_n^{(2)}$. Similar to (2.17), the formula can be approximated by the following form:

$$\hat{w}_n^{(2)} \cong \sum E\left[w_n^{(2)} \middle| \underline{I}_n^{n-\mu+1}\right] P\left(\underline{I}_n^{n-\mu+1} \,\middle|\, \underline{J}_{n-d}\right), \tag{3.2}$$

where the summation is over all the possible μ-fold sequences of $\underline{I}_n^{n-\mu+1}$. In (3.2), $E\left[w_n^{(2)} \middle| \underline{I}_n^{n-\mu+1}\right]$ is a codebook, and the probability part can be computed as explained in Section 3.2.2. The estimated complex antenna weight should have a constant amplitude. Hence, according to Lemma 1, the antenna weight can be calculated using the MMSE solution of (3.1) or (3.2) as

$$\hat{w}_n^{(2)\,normal} = \frac{1}{\sqrt{2}} \frac{\hat{w}_n^{(2)}}{\left|\hat{w}_n^{(2)}\right|}. \tag{3.3}$$

3.2.2 Markov Model

For capturing the residual redundancies [42] in the feedback stream, we assume that the bitstream follows a Markov model of order γ. A trellis structure is set up based on the Markov model to exploit the redundancies. The states of the trellis are defined as $S_n = \underline{I}_n^{n-\gamma+1}$. The trellis is specified by the probabilities of the state transitions, $P(S_n|S_{n-1})$, which are the A Priori Probabilities (APP) of the Markov model.

3.2.3 Calculation of the A Posteriori Probabilities at Transmitter

The probability $P\left(\underline{I}_n^{n-\mu+1} \,\middle|\, \underline{J}_{n-d}\right)$ in (3.2) could be calculated by using the state probabilities given the received feedback data, $P(S_n|\underline{J}_{n-d})$. In the absence of feedback delay, this calculation reduces to $P(S_n|\underline{J}_n)$ as in the previous chapter which is the estimation of the state probabilities at time n given the feedback symbols up to time n. In the following, we present a recursive algorithm for calculation of $P(S_n|\underline{J}_{n-d})$. Note that this formulation has a predictive nature as well, because the last d feedback symbols are not available due to the feedback delay. In other words, this is a joint prediction and estimation method, and so the resulting algorithm is called *SoftNMMSE-JP*, where *JP* stands for Joint Prediction.

Let

$$\begin{aligned} P(S_n|\underline{J}_{n-d}) &= C_1 \cdot P(S_n, \underline{J}_{n-d}) \\ &= C_1 \cdot P(\underline{J}_{n-d-1}) \cdot P(S_n|\underline{J}_{n-d-1}) \\ &\quad \cdot P(J_{n-d}|S_n, \underline{J}_{n-d-1}) \qquad (3.4) \\ &= C_2 \cdot P(S_n|\underline{J}_{n-d-1}) \cdot P(J_{n-d}|I_{n-d}) \qquad (3.5) \end{aligned}$$

for $d \leq \gamma - 1$, where C_1 and C_2 are normalizing variables. The term $P(S_n|\underline{J}_{n-d-1})$

can be written as follows

$$\begin{aligned} P(S_n|\underline{J}_{n-d-1}) = & \\ & \sum_{\underline{S}_{n-1}} \cdots \sum P(S_n|\underline{S}_{n-1}, \underline{J}_{n-d-1}) \cdot P(\underline{S}_{n-1}|\underline{J}_{n-d-1}) \\ = & \sum_{\underline{S}_{n-1}} \cdots \sum P(S_n|S_{n-1}) \cdot P(S_{n-1}, \underline{S}_{n-2}|\underline{J}_{n-d-1}) \\ = & \sum_{S_{n-1}} P(S_n|S_{n-1}) \cdot \sum_{\underline{S}_{n-2}} \cdots \sum P(S_{n-1}, \underline{S}_{n-2}|\underline{J}_{n-d-1}) \\ = & \sum_{S_{n-1}} P(S_n|S_{n-1}) \cdot P(S_{n-1}|\underline{J}_{n-d-1}). \end{aligned} \tag{3.6}$$

Therefore, $P(S_n|\underline{J}_{n-d})$ can be calculated recursively as

$$\begin{aligned} P(S_n|\underline{J}_{n-d}) = & C_2 \cdot P(J_{n-d}|I_{n-d}) \\ & \cdot \sum_{S_{n-1}} P(S_n|S_{n-1}) \cdot P(S_{n-1}|\underline{J}_{n-d-1}). \end{aligned} \tag{3.7}$$

Another approach to overcome the feedback delay is introduced in the following section.

3.2.4 Channel Prediction at the Receiver

If the receiver calculates the feedback symbols by using the future channel states, it can cancel out the effect of the delay in the feedback channel. This approach can be implemented by using d-step predicted values of the channel coefficients, and these values can be computed by applying a short-range fading prediction algorithm [15, 55, 56] to the current channel values. Here we use an Auto Regressive (AR) model of order 3 to predict the fading samples, and *SoftNMMSE* is used to deal with the feedback error. The resulting algorithm is called *SoftNMMSE-LP* where *LP* stands for Linear Prediction.

In practice, channel coefficients are estimated using some pilots, training bits, etc. which usually introduce some error in the available channel coefficients. Note that these channel estimates are used to generate feedback symbols, calculate the LLR values for the decoding process, etc. Therefore, the quality could have a direct impact on the overall performance of a closed-loop system. Here, the channel estimation error is modeled as an Additive White Gaussian Noise (AWGN), and SNR_z is defined as the ratio of the average channel fading power, $E[|h_n|^2]$, to the noise power. The effect of SNR_z on the performance of different algorithms is examined in the simulations.

3.3 Antenna Weight Verification

Section 2.4 explains the two effects of the feedback error on the performance. To minimize the mismatch effect, a technique called Antenna Weight Verification (AV) has been suggested as explained in Section 2.4.1. In this method, some extra preamble bits are transmitted to each user. These bits are used to estimate the dedicated channel which includes the effect of possible feedback errors. The drawbacks of using AV techniques are the need for the preamble bits for each user, and the extra complexity at the mobile unit.

In the next section, we introduce a novel technique called Blind Antenna Verification (BAV) which does not need any extra preamble bits. This blind method processes the feedback symbols, which means that the proposed method has a low complexity in comparison with symbol-based[1] blind approaches (such as the blind

[1]By a symbol-based method, we mean that a method that needs to perform calculations on the sequence of data symbols. On the other hand, the proposed method in this chapter only needs a slot-by-slot calculation. The complexity of these two approach is proportional to symbol rate and feedback rate, respectively.

antenna selection verification methods introduced in [54]). Using the proposed BAV in conjunction with the *SoftNMMSE-JP* algorithm provides an efficient closed-loop algorithm in the presence of feedback imperfections, as shown in the numerical results.

3.3.1 Blind Antenna Verification

Consider Fig. 2.7. At the transmitter, the best estimate of the optimum beamforming weight, in the MMSE sense, is

$$\hat{\mathbf{w}}_n = E[\mathbf{w}_n | \underline{J}_{n-d}]. \tag{3.8}$$

Transmitter applies the weight to the transmit signals. At the receiver, an estimate of $\hat{\mathbf{w}}_n$ is required for the decoding process, for example, for the calculation of v in (2.12). Assume that the receiver uses $\tilde{\mathbf{w}}_n$. Hence, $\tilde{\mathbf{w}}_n$ needs to be as close to $\hat{\mathbf{w}}_n$ as possible. In the following, we introduce a theorem to address this problem. Two lemmas are introduced beforehand which are used to prove the theorem.

Lemma 2. *The following sequence*

$$\mathbf{w}_n \leftrightarrow \underline{I}_{n-d} \leftrightarrow \underline{J}_{n-d} \tag{3.9}$$

constitutes a Markov chain.

Proof. See Appendix C. □

Lemma 3. *Assume that $X \leftrightarrow Y \leftrightarrow Z$ constitutes a Markov chain. Then,*

$$E\left[E[X|Y]|Z\right] = E[X|Z]. \tag{3.10}$$

Proof. See Appendix D. □

Note that the inner $E[\cdot]$ of the left side of (3.10) and the $E[\cdot]$ of the right side are with respect to X, and the outer $E[\cdot]$ of the left side is with respect to Y.

Theorem 1 (Joint Beamforming and Blind Antenna Verification)**.** *In a closed-loop system, the following criteria are desired:*

1. *Select* $\tilde{\mathbf{w}}_n$ *to*

$$\text{minimize } E\|\tilde{\mathbf{w}}_n - \mathbf{w}_n\|^2 \tag{3.11}$$

given $\underline{I}_{n-d}$ *which is available at the receiver.*

2. *Select* $\hat{\mathbf{w}}_n$ *to*

$$\text{minimize } E\|\hat{\mathbf{w}}_n - \tilde{\mathbf{w}}_n\|^2 \tag{3.12}$$

given $\underline{J}_{n-d}$ *which is available at the transmitter.*

The following system satisfies both criteria:

$$\tilde{\mathbf{w}}_n = E[\mathbf{w}_n|\underline{I}_{n-d}], \tag{3.13}$$

$$\hat{\mathbf{w}}_n = E[\mathbf{w}_n|\underline{J}_{n-d}]. \tag{3.14}$$

Proof. From criterion 1, according to the fundamental theorem of estimation (3.13) is obtained. The transmitter should find an estimate of $\tilde{\mathbf{w}}_n$ as given in (3.12). Let us call this weight $\hat{\tilde{\mathbf{w}}}_n$. Again, by using the fundamental theorem of estimation, from criterion 2 we can write

$$\hat{\tilde{\mathbf{w}}}_n = E[\tilde{\mathbf{w}}_n|\underline{J}_{n-d}]. \tag{3.15}$$

In the following, we will show that $\hat{\tilde{\mathbf{w}}}_n = \hat{\mathbf{w}}_n$ where $\hat{\mathbf{w}}_n$ is introduced in (3.14), and this concludes the proof.

According to Lemma 2,

$$\mathbf{w}_n \leftrightarrow \underline{I}_{n-d} \leftrightarrow \underline{J}_{n-d} \tag{3.16}$$

constitutes a Markov chain. Hence we can write

$$\hat{\tilde{\mathbf{w}}}_n = E[\tilde{\mathbf{w}}_n|\underline{J}_{n-d}] \tag{3.17}$$

$$= E\left[E[\mathbf{w}_n|\underline{I}_{n-d}]\,\middle|\,\underline{J}_{n-d}\right] \tag{3.18}$$

$$= E[\mathbf{w}_n|\underline{J}_{n-d}] \tag{3.19}$$

$$= \hat{\mathbf{w}}_n, \tag{3.20}$$

where Lemma 3 is used to derive (3.19). The result shows that if the transmitter uses (3.14), and the receiver uses (3.13), both criteria are satisfied. □

Note that theorem 1 does not explicitly use the optimal beamforming criterion (i.e., minimize $E\|\hat{\mathbf{w}}_n - \mathbf{w}_n\|^2$, as is used in the previous chapter), however this criterion is satisfied by (3.14). This means that beamforming goal and AV goal are jointly achieved by using the theorem. This method does not need any dedicated (i.e., user-specific) training sequence at the receiver and so it is a blind solution for the AV problem. For the implementation of the solution introduced in Theorem 1, the receiver calculates (3.13) which could be done similar to (3.2). However, it does not need any trellis processing because the probabilities are fixed. The required $P(S_n|\underline{I}_{n-d})$ can be calculated as shown in Appendix E.

3.4 Numerical Results

The block diagram of the simulated feedback system is shown in Fig. 2.7. The simulation parameters are summarized in Table 2.5. The feedback bitstream is BPSK

modulated (uncoded) and added with White Gaussian Noise with the variance of $\sigma_n^2 = 0.370$ (equivalent to the feedback error of 5%). A feedback delay $D = 2$ is assumed. The following algorithms are compared: *Standard*, *SoftNMMSE-JP-BAV*, *SoftNMMSE-LP*, and *SoftNMMSE-IP*. *Standard* refers to the closed-loop mode 1 of the 3GPP standard, as explained in Section 2.3. The algorithm *SoftNMMSE-JP-BAV* is an implementation of Theorem 1 which is a combination of the Joint Prediction approach of Section 3.2 and Blind Antenna Verification. The algorithm *SoftNMMSE-LP* uses the approach in Section 3.2.4 which applies a linear predictor of order 3 for channel prediction. Finally, the algorithm *SoftNMMSE-IP* (where "*IP*" stands for Ideal Channel Prediction) uses the same approach as Section 3.2.4, but assumes that the required future channel coefficients are perfectly available without the effect of channel estimation and channel prediction errors. Therefore, *SoftNMMSE-IP* can be considered as a performance bound for dealing with feedback delay. It is notable that *SoftNMMSE-JP-BAV* and *SoftNMMSE-LP* are enhancements to the closed-loop mode 1 of 3GPP, and they are compatible with the standard.

Figs. 3.1 - 3.2 show the FER performance curves versus transmit SNR at four different mobile speeds (V=1, 5, 25, and 100 kmph), for $\text{SNR}_z = 40$ dB representing the case where the channel estimation has a good quality (for example, when powerful channel pilots are available). Similarly, Figs. 3.3 - 3.4 shows the FER performance curves for $\text{SNR}_z = 10$ dB representing the case with poor channel estimation quality (for example, when blind channel estimation is used at the receiver).

It is observed that both proposed approaches significantly outperform the *Standard* algorithm at all mobile speeds. For the case of high SNR_z, the channel prediction approach acts better than the joint approach which only uses the feedback bitstream.

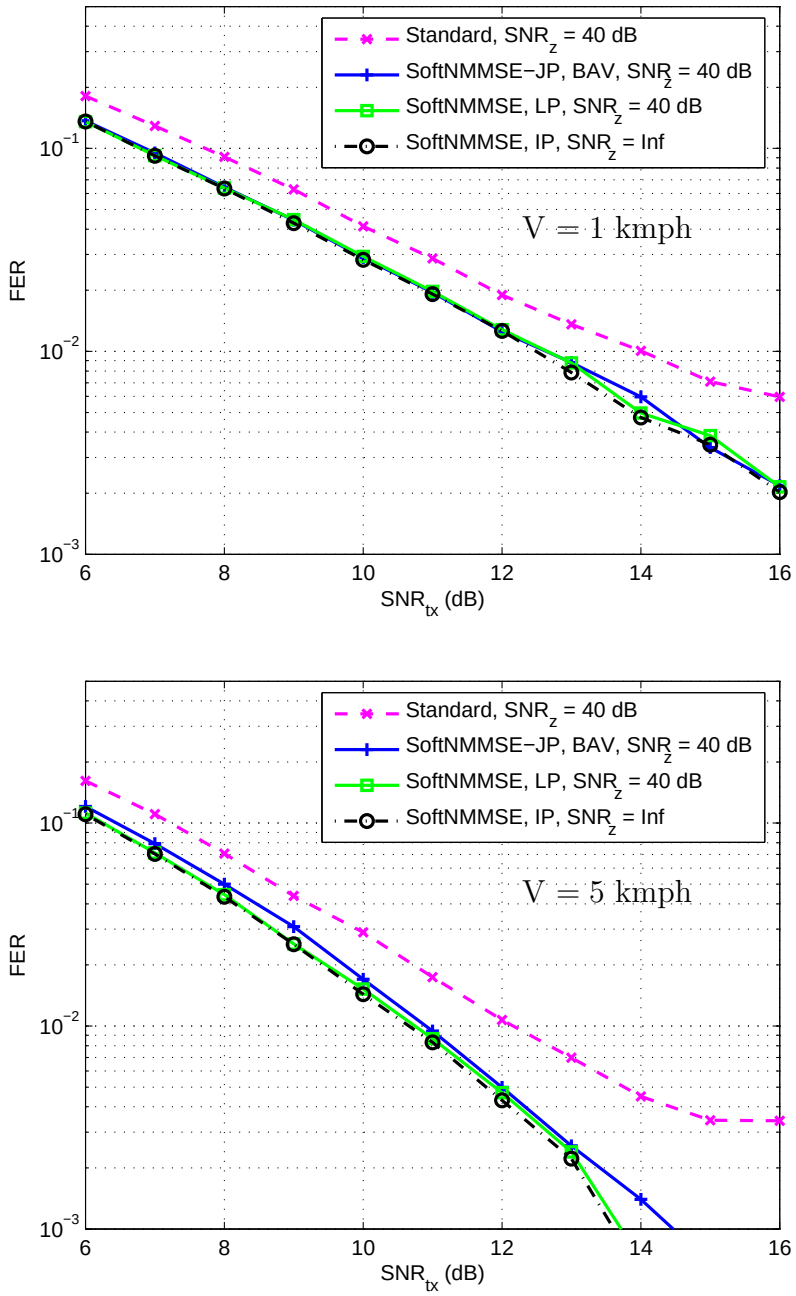

Figure 3.1: FER performance at $\mathrm{SNR}_z = 40\,\mathrm{dB}$ for $\mathrm{V} = 1$ and 5 kmph

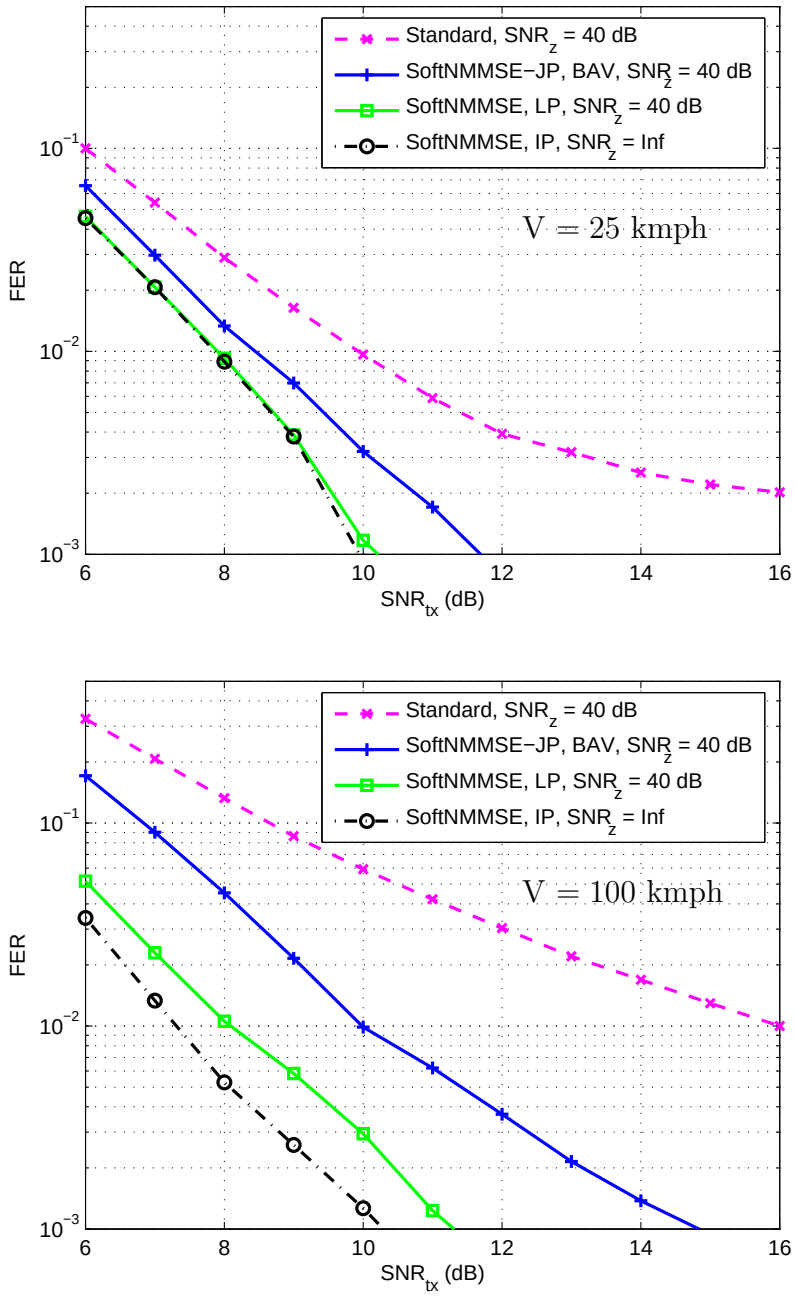

Figure 3.2: FER performance at $\mathrm{SNR}_z = 40\,\mathrm{dB}$ for $\mathrm{V} = 25$ and 100 kmph

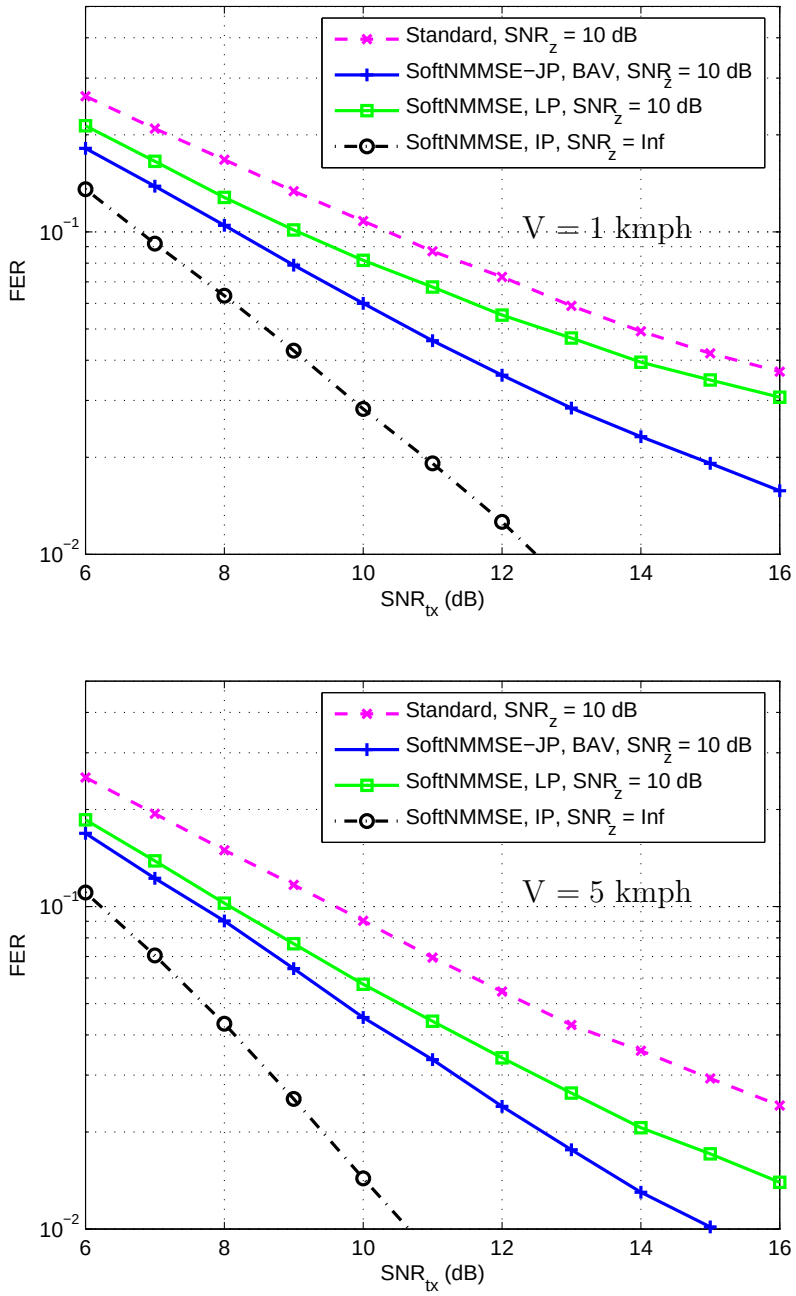

Figure 3.3: FER performance at $\mathrm{SNR}_z = 10\,\mathrm{dB}$ for $\mathrm{V} = 1$ and 5 kmph

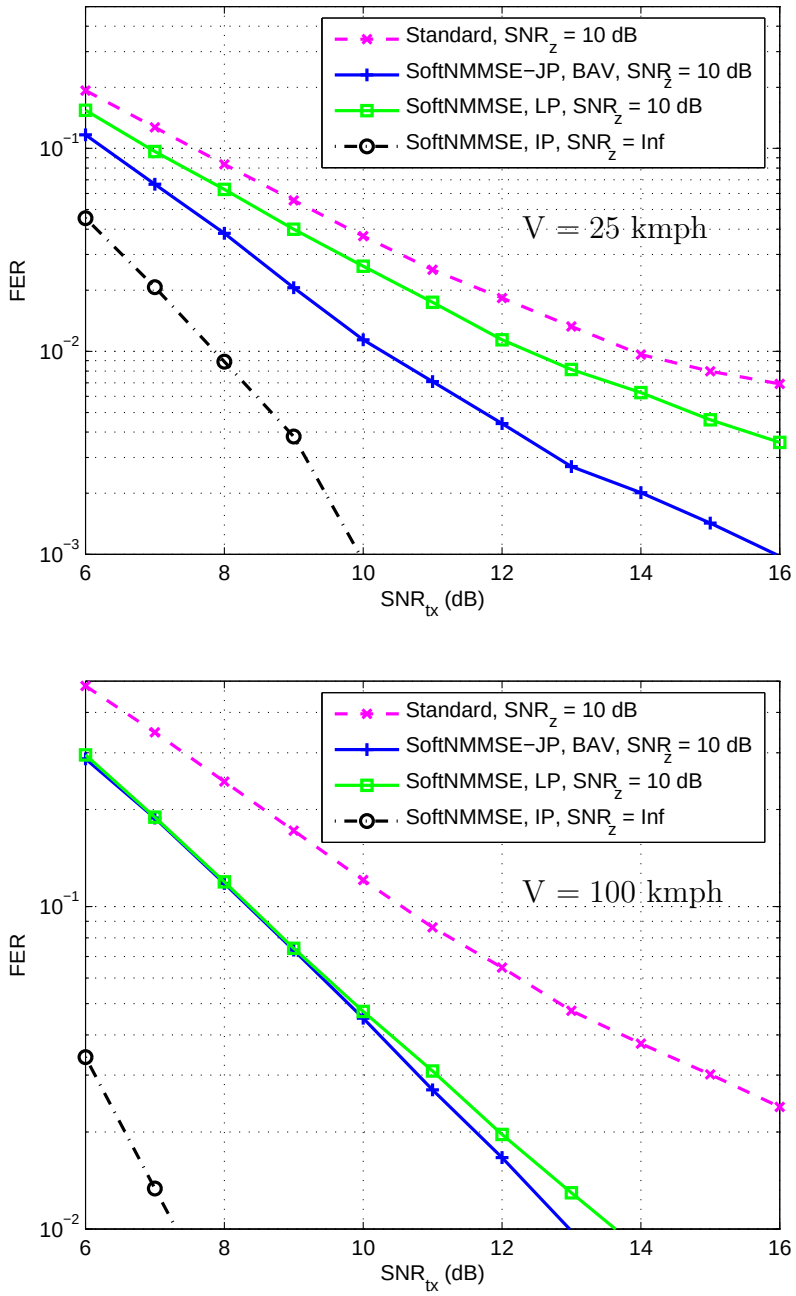

Figure 3.4: FER performance at $\mathrm{SNR}_z = 10\,\mathrm{dB}$ for $\mathrm{V} = 25$ and 100 kmph

However, when SNR_z is low, the joint approach acts better, since the predicted channel values are not very accurate in this case.

For high SNR_z and low mobile speeds, both approaches have the same performance and offer about 1 dB gain over the *Standard* algorithm. When the mobile speed is low, channel is changing slowly and the roughly quantized CSI has enough information about the channel. Also, the channel prediction algorithms act very well as the channel values have significant time-correlation. In other words, the effect of feedback delay vanishes for low mobile speeds. Therefore, as it is observed in Fig. 3.1 for V=1 kmph, both approach touch the "*SoftNMMSE-IP*" performance. As the mobile speed increases (and/or for larger feedback delays), the increasing effect of feedback delay causes the performance curves to split.

It is observed that at high mobile speeds, our joint approach significantly outperforms the *Standard* algorithm, for both poor and good quality of channel estimation. This shows that our joint prediction algorithm can be used to increase the range of mobile speeds where the closed-loop algorithm can be effectively applied. The algorithm only needs the calculations once per each feedback slot (i.e., the total complexity is proportional to the feedback rate which is much less than the data symbol rate), and the algorithm has a reasonable complexity, mostly needed at the base station. Both approach proposed in this chapter are similarly applicable to any other MIMO closed-loop system.

3.5 Conclusion

The performance of the closed-loop transmit diversity is limited, which is the result of the rate limit, delay, and error in the feedback channel and also the non-optimum

weight reconstruction algorithms. In this chapter, we propose two approaches to improve the performance of the closed-loop system, particularly in the presence of feedback delay. We address the problem of the decoding mismatch at the receiver by proposing a Blind Antenna Verification algorithm. It is shown in a theorem that using the optimal reconstruction at the transmitter and the blind antenna verification algorithm (at the receiver) is a jointly optimal approach to achieve the beamforming goal and the antenna verification goal. A number of algorithms are introduced, and it has been shown that our algorithms can provide significant gains over the conventional method at all mobile speeds, and also for both good and poor quality of the channel estimation at the receiver.

Chapter 4

Modeling and Prediction of Fading Channels

A key element for many fading-compensation techniques is a (long-range) prediction tool for the fading channel. A linear approach, usually used to model the time evolution of the fading process, does not perform well for long-range prediction applications. In this chapter, we propose an adaptive channel prediction algorithm using a state-space approach for the fading process based on the sum-sinusoidal model. Also to enhance the popular linear approach, we propose a tracking method for a multi-step linear predictor. Comparing the two methods in our simulations show that the proposed algorithm significantly outperforms the linear method, for both stationary and non-stationary fading processes, especially for long-range predictions. The self-recovering structure, as well as the reasonable computational complexity, makes the proposed algorithm appealing for practical applications[1].

[1]The material presented in this chapter has partly been filed as a patent [57].

4.1 Introduction

In this chapter, we address the problem of channel fading modeling and prediction. Channel fading prediction can be used to improve the performance of telecommunication systems. Having estimates of future samples of the fading coefficients enhances the performance of many tasks at the receiver and/or at the transmitter, including adaptive coding and modulation, channel equalization, the decoding process of data symbols, and antenna beamforming. In particular, the performance of adaptive coding and modulation techniques strongly depends on the performance of the fading prediction algorithm [14], and usually a long-range prediction algorithm is required [15]. The prediction tool even allows applying non-causal algorithms to optimize the closed-loop schemes. Another application of the fading prediction is to compensate for the effect of feedback delay in closed-loop communication systems [16]. An extensive literature survey on the subject of fading modeling and prediction can be found in [15].

Consider a single-path[2] flat fading channel from a transmit antenna to a receive antenna. The channel fading coefficient h_n is zero mean (subscript n is the time index), with the variance $\sigma_h^2 = 1$. Fig. 4.1 shows the block diagram for prediction of a fading channel. The channel coefficients are estimated from the received signal series $\{y_n\}$, where the nature of y_n could be different depending on the application. Usually y_n is a pilot signal which is appropriately designed for channel estimation, as in 3G systems. In some applications, y_n is the modulated user data which is used by a blind channel estimation algorithm. The subject of channel fading estimation

[2]If the path delay variations are not negligible in comparison with the symbol period, the same analysis could be applied to each resolved multipath component.

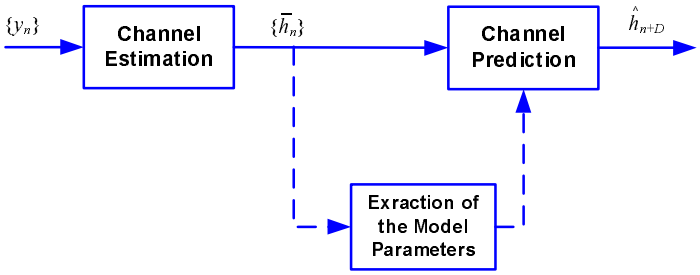

Figure 4.1: The general block diagram of a channel prediction scheme

is well-established in the literature and will not be addressed here. We assume that the channel estimate $\overline{h}_n$ is shown as $\overline{h}_n = h_n + v_n$, where v_n is the estimation error modeled as a zero mean Gaussian noise [58] with the variance σ_v^2. As an indicator for the estimation quality, the observation SNR is defined (like the previous chapter) as $\text{SNR}_z = \sigma_h^2/\sigma_v^2 = 1/\sigma_v^2$.

For prediction of a future sample of the channel using the past measurements, a model is needed to represent the dynamics of the channel. Having the series of the channel measurements $\{\overline{h}_n\}$, the parameters of the model are estimated or updated, and the future fading sample is predicted as shown in Fig. 4.1. The model selection and extraction of the parameters, as well as the prediction algorithm, are explained in the sequel.

Many processes are represented with a linear model, i.e. an auto-regressive moving-average (ARMA) model. In this context, an approximate low-order AR model is often used as it can capture most of the fading dynamics. For example, see the MMSE linear predictor proposed in [59], and the channel tracking algorithms utilizing Kalman filter in [60] and [61]. Linear models are known to be optimal for Gaussian signals. Also linear models are easy to use and have a low complexity, however, they fail to show the true time behavior of a channel fading process. The Gaussian assumption

for the fading signal is only valid for a rich-scattering area, i.e., when the number of dominant scatterers are significant. However, in many mobile environments, there are a few main scatterers which construct the fading signal [18]. Also the time-varying nature of the fading signal is in contrast with the Gaussian assumption in any case. Overall, the linear models do not perform well for long-range predictions as shown in the literature (for example, see [62]). The block-adaptive linear predictors are widely used, however for a fast time-varying channel (or for a long block length), the model parameters become outdated towards the block end. This problem can be ratified to some extent by updating the linear coefficients more frequently using adaptive methods [15]. Other than the linear approach, some other prediction approaches have been used for fading channels. Article [62] uses a (nonlinear) quadratic approach and shows that while it has good modeling properties, it is very sensitive to the model changes. Nonlinear methods have usually high complexities and they are hard to analyze. Furthermore, they are usually difficult to be adaptively applied. In this work, we utilize a nonlinear model as explained in the following. By applying an equivalent state-space model, we avoid the problems of nonlinear processing.

When the receiver, the transmitter, and/or the scatterers are moving, each scattered component undergoes a doppler frequency shift given approximately by [19]

$$f(k) = f_d \cos(\theta(k)) \tag{4.1}$$

where $\theta(k)$ is the incident radiowave angle of the k'th component with respect to the motion of the mobile and f_d is the maximum doppler frequency defined as $f_d = \frac{V}{C} f_c$, where f_c is the carrier frequency, V is the mobile speed and C is the speed of light. Assuming N_{sc} scatterers, the complex envelop of the flat fading signal at the receiver

is

$$h(t) = \sum_{k=1}^{N_{\rm sc}} \rho(k)\, e^{j(\omega(k)\, t + \phi(k))} + \zeta(t) \tag{4.2}$$

where for the k'th scatterer, $\rho(k)$ is the (real) amplitude, $\phi(k)$ is the initial phase, $\omega(k) = 2\pi f(k)$, and $\zeta(t)$ is the model error. The phase $\phi(k)$ can be absorbed in the amplitude as $\alpha(k) = \rho(k)\, e^{j\phi(k)}$. According to (4.2), a fading channel can be modeled as sum of a number of sinusoids. This so-called sum-sinusoidal model relies on the physical scattering mechanism [17]. Previously, this model has been used for prediction of the channel fading [63, 64, 65, 66]. In this work, we use the sum-sinusoidal model in a Kalman filtering framework. This model is *adaptively* updated [67] to follow the changes in the scattering environment. Unlike most of the works in the literature, we propose a complete adaptive modeling and prediction algorithm for time-varying fading channels. Also we present an enhanced adaptive linear algorithm, then compare their performance. It is shown here how these two approach perform in a real situation with practical assumptions.

Assuming a two-dimensional isotropic scattering and an omni-directional receiving antenna, it is known that the autocorrelation function of the fading process can be written as [17]

$$R_h(t, t-\tau) = \frac{E[h(t)h^*(t-\tau)]}{\sigma_h^2} = J_0(2\pi f_d \tau), \tag{4.3}$$

where f_d is the maximum doppler frequency, $J_0(\cdot)$ is the first-kind Bessel function of the zero order, and τ is the time difference. A Rayleigh fading process with the above correlation property is called the Jakes fading [17, 27]. We examine the performance of the algorithms with the Jakes fading, and also with a non-stationary fading which is generated by a ray-tracing approach.

In the next two sections, the linear approach and the proposed approach are

presented. Then, the algorithms are compared in the simulation results.

4.2 Linear Approach

To model a fading process, a linear model is widely used. An AR (Auto Regressive) model of order N_{AR} is recursively defined as follows

$$h_{n+1} \;=\; \sum_{i=1}^{N_{\mathrm{AR}}} a(i)\, h_{n-i+1} + \xi_{n+1} \tag{4.4}$$

where $\mathbf{a} = [a(1),\, a(2),\, \cdots,\, a(N_{\mathrm{AR}})]^T$ is the AR coefficients vector, and ξ_{n+1} is the model error which has a zero mean.

The time evolution of an AR model can also be shown as a state-space model [60, 68] as follows

$$\begin{cases} \mathbf{h}_n = \mathbf{B}\,\mathbf{h}_{n-1} + \mathfrak{q}_n \\ z_n = \mathfrak{m}\,\mathbf{h}_n + u_n \end{cases} \tag{4.5}$$

where

$$\mathbf{h}_n = [h_n,\, h_{n-1},\, \cdots,\, h_{n-N_{\mathrm{AR}}+1}]^T \tag{4.6}$$

is the fading regressor at time n, $\mathbf{B}$ is the transition matrix defined as

$$\mathbf{B} = \begin{pmatrix} & \mathbf{a}^T & \\ \mathbf{I}_{N_{\mathrm{AR}}-1 \times N_{\mathrm{AR}}-1} & & \mathbf{0}_{\mathbf{N_{AR}-1\times 1}} \end{pmatrix}, \tag{4.7}$$

and $\mathfrak{q}_n$ is the noise vector defined as $\mathfrak{q}_n = [\xi_n,\, \xi_{n-1},\, \cdots,\, \xi_{n-N_{\mathrm{AR}}+1}]^T$ representing the model error. $\mathfrak{m}$ is known as the measurement matrix which is defined as

$$\mathfrak{m} = [1,\, 0,\, \cdots,\, 0]_{1\times N_{\mathrm{AR}}}, \tag{4.8}$$

u_n is the observation noise, and z_n is the system output (which is substituted by the observed values for implementation).

It is easy to show that

$$\hat{\mathbf{h}}_{n+1|n} = \mathbf{B}\,\mathbf{h}_n, \tag{4.9}$$

where $\hat{\mathbf{h}}_{n+1|n}$ is the prediction of $\mathbf{h}_{n+1}$ given the observations up to the time n, i.e., $\hat{\mathbf{h}}_{n+1|n} = E\left[\mathbf{h}_{n+1}|z_n,\, z_{n-1}\,\cdots\right]$.

4.2.1 The Linear Prediction Algorithm (LP)

Assuming an AR model of the order N_{AR}, a 1-step linear predictor is shown as follows

$$\hat{h}_{n+1|n} \;=\; \sum_{i=1}^{N_{\mathrm{AR}}} a(i)\,\overline{h}_{n-i+1}, \tag{4.10}$$

where $\overline{h}_n$ is the channel estimate as defined before. Minimizing the mean square error (MSE), $E\left[\left|h_{n+1} - \hat{h}_{n+1|n}\right|^2\right]$, provides the prediction coefficients $\mathbf{a}$ via solving the Yule-Walker equations [69].

For the Jakes fading, $\mathbf{a}$ is analytically available [70]. In practice, $\mathbf{a}$ is estimated using the fading samples using one of the well-known methods such as Levinson method, Burg method, or Prony method. In a non-stationary environment, the coefficients are frequently updated to follow the model variations.

Here, the linear coefficients are estimated using a Least-Squares approach and solving the equations by the Levinson-Durbin recursion over a window length of T_{AR}. The estimates are updated every T_{AR} samples. Fig. 4.2 shows the flowchart of the algorithm.

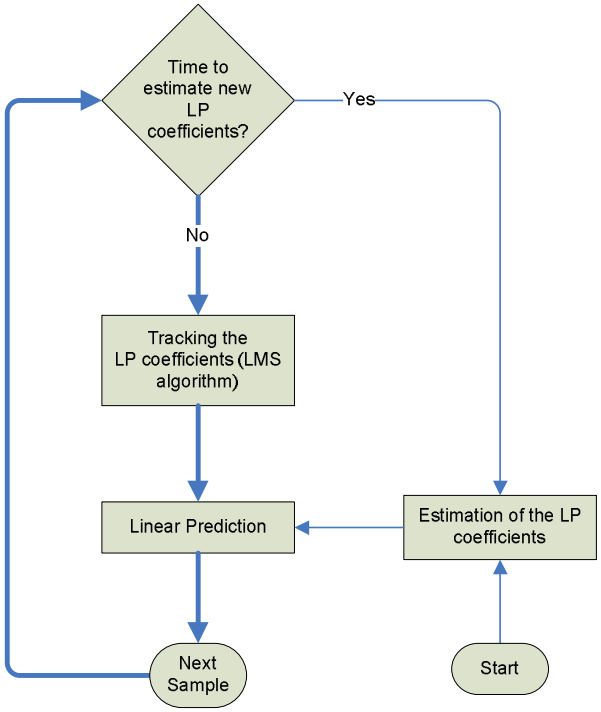

Figure 4.2: Block diagram of the linear prediction algorithm (LP)

4.2.2 D-step Versus 1-step Prediction

To perform a D-step prediction, the 1-step predictor could be used D times recursively. However, we are interested in a direct D-step prediction method because it is easier to analyze and to implement. Furthermore, this is particularly helpful in the tracking mode as it is addressed in Section 4.2.3. Equation (4.10) can be extended to provide a D-step linear predictor as follows

$$\hat{h}_{n+D|n} = \sum_{i=1}^{N_{\mathrm{AR}}} a^{(D)}(i)\, \overline{h}_{n-i+1}. \tag{4.11}$$

The superscript "(D)" indicates that the variable is related to the D-step predictor. Calculation of the coefficients of the 1-step predictor, $\mathbf{a}$, was explained before. For the D-step predictor,

$$\mathbf{a}^{(D)} = [a^{(D)}(1),\ a^{(D)}(2),\ \cdots,\ a^{(D)}(N_{\mathrm{AR}})]^T \tag{4.12}$$

can be computed using $\mathbf{a}$. From the state-space model, it is shown [71] that $\hat{\mathbf{h}}_{n+D|n} = \mathbf{B}^D\, \mathbf{h}_n$, similar to (4.9). Hence,

$$\hat{h}_{n+D|n} = \mathfrak{m}\, \hat{\mathbf{h}}_{n+D|n} \tag{4.13}$$

$$= \mathfrak{m}\, \mathbf{B}^D\, \mathbf{h}_n. \tag{4.14}$$

By comparing (4.14) and (4.11) it is observed that $\mathbf{a}^{(D)} = (\mathfrak{m}\, \mathbf{B}^D)^T$, meaning $\mathbf{a}^{(D)^T}$ is the first row of $\mathbf{B}^D$. Therefore, to obtain the coefficients of the D-step predictor, the calculation steps are as follows:

$$\mathbf{a} \rightarrow \mathbf{B} \rightarrow \mathbf{B}^D \rightarrow \mathbf{a}^{(D)} \tag{4.15}$$

4.2.3 Tracking

In a non-stationary environment, the model is changing and the assumption of a fixed model over the observation window results in a performance degradation. A low-complexity adaptive algorithm is desired to track the changes of $\mathbf{a}_n$ over time. An LMS algorithm is used as in [15]

$$\mathbf{a}_{n+1} = \mathbf{a}_n + \mu_{\text{AR}}\, \mathbf{h}_n^H\, e_n \tag{4.16}$$

where $e_n = h_n - \hat{h}_n$. Note that we have added the time index n for $\mathbf{a}_n$ in the tracking mode signifying that it is changing at each time step.

As explained in Section 4.2.2, $\mathbf{a}_n^{(D)}$ is calculated using $\mathbf{a}_n$, which requires the calculation of $\mathbf{B}_n^D$. In the tracking mode, this calculation is needed whenever $\mathbf{a}_n$ is updated, which can impose a high computational complexity. In Appendix F, we propose a method to decrease the complexity. Using this method, the final equation for tracking a D-step linear predictor is similar to the LMS algorithm of (4.16), and is as follows

$$\mathbf{a}_{n+1}^{(D)} = \mathbf{a}_n^{(D)} + \mu_{\text{AR}}\, \mathbf{G}_n^{(D)}\, \mathbf{h}_n^H\, e_n, \tag{4.17}$$

where $\mathbf{G}_n^{(D)}$ is an $N_{\text{AR}} \times N_{\text{AR}}$ matrix. Appendix F explains the structure and the calculation of $\mathbf{G}_n^{(D)}$.

4.3 The Proposed Approach

Consider the fading model shown in (4.2). Assuming a sampling rate of $f_s = 1/T_s$, the fading samples can be written as

$$h_n = \sum_{k=1}^{N_{\text{sc}}} \alpha(k)\, e^{j\omega(k) n T_s} + \zeta_n \tag{4.18}$$

where $h_n = h(nT_s)$, and n is the time index. In many mobile environments, there are a few main scatterers which construct the fading signal [18]. Whereas in some urban areas there could be up to eight or even more contributing components in the fading signal [72]. In any case, the sum-sinusoidal model of (4.18) can represent the fading signal. Note that the Jakes model is a special case of the sum-sinusoidal model, and is mathematically valid only for a rich-scattering environment.

4.3.1 Estimation of the Model Parameters

Estimation of the parameters of a sum-sinusoidal model is a well-known problem [73], particularly in the areas like acoustic and speech processing, and signal processing in communications. In this work, we are interested in a practical and efficient solution with complexity constraints, for modeling the mobile fading channel.

A majority of the works on channel modeling use a statistical approach to capture the channel behavior. However, the fading model (4.18) could be observed as a deterministic equation, and a handful of articles have used this approach to capture the behavior of the fading process, e.g., refer to [63, 64, 65, 66]. Assuming N_{sc} scatterers, there are $2\,N_{\text{sc}}$ unknown parameters to be determined in the model given in (4.18). As a systematic solution, only $2\,N_{\text{sc}}$ fading samples are required to form an equation set. Solving the equation set provides $\omega(k)$ and $\alpha(k)$, for $k = 1, \cdots, N_{\text{sc}}$. As this approach uses only a few noisy measurements of the fading process, it could result in poor estimation of the parameters. Article [64] uses an ESPIRIT algorithm to find the doppler frequencies, and then solves a set of linear equations using the Least-Squares method to estimate the complex amplitudes. Alternatively, article [63] uses the Root-MUSIC method to find the doppler frequencies. To estimate the amplitudes,

the Least Squares and the Bayesian methods are used in [65] assuming that the doppler frequencies are known. As another solution, [65] assumes an AR model for each $\alpha(k)$, estimates the AR coefficients using a Modified Covariance method, and constructs a Kalman filter on the AR model to estimate the amplitudes [65].

In this chapter, we propose a new approach to estimate and track the parameters. We utilize the fact that the doppler frequencies usually change slower compared to the complex amplitude variations when the setting of the scattering environment is the same. Generally speaking, this is because the doppler frequency variations are the result of any acceleration of the mobile movement, however the complex amplitudes change even when the mobile is moving at a constant velocity as the distances are changing. Therefore, we separate the tracking of $\omega(k)$'s and $\alpha(k)$'s which have different dynamics. The details of the proposed method follows.

Assuming a constant scattering model, the Fourier transform of the fading signal shown in (4.18) can provide the estimates of the model parameters, as different scattering components are decoupled in the frequency domain. Fourier analysis can provide an accurate estimation of $\omega(k)$'s if they do not change significantly and the observation window is not too short. In practice, the $\omega(k)$'s change slowly with time. Therefore, a high-resolution method is required to estimate the doppler frequencies using a short window of recent measurements, as in [63, 64, 65]. Furthermore, these estimates need to be performed frequently which imposes a high computational complexity. However, this problem can be solved by an adaptive filter. We utilize a tracking loop to follow the slow variations of $\omega(k)$'s at each fading sample. Therefore, unlike the window-based methods, the doppler frequencies are up-to-date at each sample. A sudden change in the frequencies may occasionally happen, for example, if

the mobile path abruptly changes. In this case, the frequencies are estimated again. Because of the robustness of this approach, the initial estimates of the frequencies do not need to be very accurate. Therefore, we can use a simple Fourier analysis to do this.

Fourier analysis can provide rough estimates for the amplitudes as well. However, $\alpha(k)$'s usually change fast, and these changes may even be significant over a few fading samples. Therefore, a vigilant algorithm is needed for tracking the $\alpha(k)$'s. Knowing $\omega(k)$'s, we construct a Kalman filter based on the sum-sinusoidal model to efficiently follow the $\alpha(k)$ variations. The state-space model is introduced in the next two sections.

4.3.2 The State-Space Model

A time evolution model is a useful tool for the prediction of a process. A well-known form of an evolution model known as the state-space model can be written as

$$\begin{cases} \mathbf{x}_n = \mathbf{A}_n \, \mathbf{x}_{n-1} + \mathbf{q}_n \\ z_n = \mathbf{m}_n \, \mathbf{x}_n + v_n \end{cases} \tag{4.19}$$

where $\mathbf{x}_n$ is an $N_{\text{ray}} \times 1$ state vector at time n, $\mathbf{A}_n$ is an $N_{\text{ray}} \times N_{\text{ray}}$ matrix which controls the transition of the state vector in time, and $\mathbf{q}_n$ is a noise vector with the covariance $\mathcal{Q}_n = E[\mathbf{q}_n \, \mathbf{q}_n^H]$, which represents the model error. The $\mathbf{m}_n$ is the measurement matrix, v_n is the observation noise, and z_n is the system output (which is substituted by the observed values for implementation). In practical systems, $\mathbf{A}_n$, $\mathcal{Q}_n$ and $\mathbf{m}_n$ are usually constant or slowly time-varying. A well-known state-space representation of an AR model can be found in Section 4.2. We propose a new state-space model for the mobile fading in the following.

Considering the sum-sinusoidal process given in (4.18), we propose the following state-space model:

$$\mathbf{A}_n = diag\left[e^{j\omega_n(1)\,T_s},\, e^{j\omega_n(2)\,T_s},\, \cdots,\, e^{j\omega_n(N_{\text{ray}})\,T_s}\right] \tag{4.20}$$

and

$$\mathbf{m}_n = [1,\, 1,\, \cdots,\, 1]_{1\times N_{\text{ray}}}, \tag{4.21}$$

where N_{ray} is the model order which is the number of the assumed scatterers (ideally, $N_{\text{ray}} = N_{\text{sc}}$). The z_n in (4.19) is substituted with the available measurement of the fading sample, i.e., $z_n = \overline{h}_n$. Therefore, the state vector $\mathbf{x}_n$ consists of the complex envelops of the scattering components. A Kalman filter can utilize the state-space model to estimate the state $\mathbf{x}_n$ at each time. An extension of this state-space model to MIMO and multipath channels is presented in Appendix G.

4.4 The Proposed Algorithm

Here we propose an adaptive algorithm for fading prediction (which is called "KF"). Fig. 4.3 shows the flowchart of the algorithm, and a description of the main blocks follows.

4.4.1 Kalman Filtering

Kalman Filtering is an estimation method which is commonly used in communication systems (for example, see [60, 74, 61]). Assuming a state-space model, Kalman filter efficiently estimates the state vector $\mathbf{x}_n$ using the observation samples. The estimation of the state vector given the observations at the time n, shown as $\mathbf{x}_{n|n}$, is optimal in

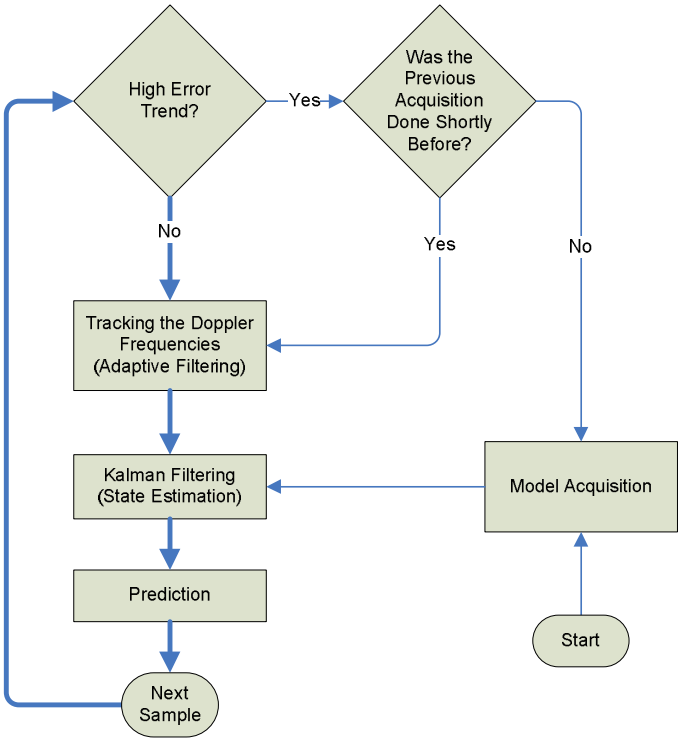

Figure 4.3: Block diagram of proposed prediction algorithm (KF)

the MMSE sense. This estimate is used to predict the future samples of the fading signal.

In the following, the Kalman equations [71] are presented, and Table 4.1 defines the variables used in the Kalman equations.

Prediction part:

$$\mathbf{x}_{n|n-1} = \mathbf{A}_n \, \mathbf{x}_{n-1|n-1} \tag{4.22}$$

$$\mathbf{P}_{n|n-1} = \mathbf{A}_n \, \mathbf{P}_{n-1|n-1} \mathbf{A}_n^T + \mathbf{Q} \tag{4.23}$$

Update part:

$$\mathbf{k}_n = \mathbf{P}_{n|n-1} \, \mathbf{m}_n^H \, \left(\mathbf{m}_n \, \mathbf{P}_{n|n-1} \, \mathbf{m}_n^H + \sigma_v^2 \right)^{-1} \tag{4.24}$$

$$\mathbf{x}_{n|n} = \mathbf{x}_{n|n-1} + \mathbf{k}_n \, \left(z_n - \mathbf{m}_n \, \mathbf{x}_{n|n-1} \right) \tag{4.25}$$

$$\mathbf{P}_{n|n} = \mathbf{P}_{n|n-1} - \mathbf{k}_n \, \mathbf{m}_n \, \mathbf{P}_{n|n-1} \tag{4.26}$$

The presented Kalman filter works properly as long as the assumed model represented by $\mathbf{A}_n$ is valid. In the transient times when the model is changing, the Kalman filter may lose the track of the state. A threshold is imposed on the magnitude of the error term in (4.25), $\epsilon_n = z_n - \mathbf{m}_n \, \mathbf{x}_{n|n-1}$, to prevent large invalid changes. Namely, if $|\epsilon_n| > T_\epsilon$ then $\epsilon'_n = T_\epsilon \, \epsilon_n / |\epsilon_n|$ is used instead. A larger threshold causes less distortion of the error signal in the tracking mode, while a smaller threshold means that the Kalman filter will converge more quickly to the new model when the scattering environment is changing. A threshold of $T_\epsilon = 4 \, \sigma_v$, selected by try and error, is used here. To decrease the transient time, the estimates of $\alpha(k)$'s from the Fourier analysis are applied as initial values to the Kalman filter.

Regarding the computational complexity, this is a low complexity Kalman filter to implement. The inversion of equation (4.24) is a scalar inversion (not a matrix

$\mathbf{Q}$	The covariance matrix of the model noise
z_n	The observation sample
$\mathbf{x}_{n\|n-1}$	The *a priori* estimate of the state $\mathbf{x}_n$ (i.e., the estimation of the state at the time n given the observations upto the time $n-1$)
$\mathbf{x}_{n\|n}$	The *a posteriori* estimate of the state $\mathbf{x}_n$ (i.e., the estimation of the state at the time n given the observations upto the time n)
$\mathbf{P}_{n\|n-1}$	The covariance matrix of the *a priori* error
$\mathbf{P}_{n\|n}$	The covariance matrix of the *a posteriori* error

Table 4.1: Variables used in the Kalman filter

inversion), and most of the other equations only need vector calculations as $\mathbf{m}_n$ is a constant vector.

4.4.2 Model Acquisition

The current parameters for the fading model are estimated according to Section 4.3.1. We apply the Fourier method to estimate $\omega(k), k = 1, \cdots, N_{\text{ray}}$ using an FFT algorithm [70].

Acquisition could be done frequently to keep up-to-date with the doppler frequency changes. To decrease the required computations, it may be done only when the scattering model has significantly changed. The proposed algorithm enters the acquisition mode when the error trend exceeds a threshold as explained in Section 4.4.5. Furthermore, the algorithm does not allow two consecutive acquisitions to happen very closely (less than T_{Acq} apart), because after each acquisition, other blocks of the algorithm need some time to converge to the new model parameters.

4.4.3 Tracking the Doppler Frequencies

An adaptive algorithm is used to track the fine changes of the doppler frequencies. Using a gradient-based approximation, the following LMS algorithm is derived in Appendix H,

$$\omega_{n+1}(k) = \omega_n(k) + \mu_{\mathrm{KF}}\, \Im\left[x^H_{n|n}(k)\, e_n\right], \tag{4.27}$$

where $\Im$ is the imaginary operator, and

$$e_n \;=\; z_n - h_{n|n} \tag{4.28}$$

is the Kalman estimation error, where

$$h_{n|n} \;=\; \mathbf{m}_n\, \mathbf{x}_{n|n}. \tag{4.29}$$

Note the entanglement of the two tracking mechanisms which avoids any possible disparity between the doppler frequencies and the amplitudes on a sample by sample basis.

4.4.4 Prediction

Given the current state $\mathbf{x}_n$, which carries all the information about the past, the future channel state should be predicted. It has been shown [71] that given a *constant* state transition matrix $\mathbf{A}_n$, the MMSE estimate of the D-step prediction is

$$\hat{\mathbf{x}}_{n+D|n} = \mathbf{A}^D_n\, \mathbf{x}_{n|n}. \tag{4.30}$$

where $\hat{\mathbf{x}}_{n+D|n}$ is the estimate of the state vector at the time $n+D$, given the observations until the time n. However, the doppler frequencies slowly change, resulting

in slight changes from $\mathbf{A}_{n+1}$ to $\mathbf{A}_{n+D}$. It is shown in Appendix I that considering the model changes over time, the optimal predictor is

$$\hat{\mathbf{x}}_{n+D|n} = \mathbf{A}_{n+D} \cdots \mathbf{A}_{n+2}\mathbf{A}_{n+1}\, \mathbf{x}_{n|n}. \tag{4.31}$$

At the time n, the matrices $\mathbf{A}_{n+2}, \cdots, \mathbf{A}_{n+D}$ are not known. However, they can be estimated by assuming the same trend for the doppler frequency changes over the next D samples. Utilizing the tracking model of (4.27), the following estimate is obtained (see Appendix J for the proof),

$$\mathbf{A}_{n+D} \cdots \mathbf{A}_{n+2}\mathbf{A}_{n+1} = \mathbf{A}_n^D \; diag[e^{j\frac{D(D+1)}{2}\delta\mathbf{w}_n T_s}], \tag{4.32}$$

where

$$\delta\mathbf{w}_n = \mathbf{w}_{n+1} - \mathbf{w}_n \tag{4.33}$$

which can be calculated using (4.27).

Using the predicted state $\hat{\mathbf{x}}_{n+D|n}$, the fading sample at the time $n+D$ can be obtained as $\hat{h}_{n+D|n} = \mathbf{m}_n\, \hat{\mathbf{x}}_{n+D|n}$.

4.4.5 Calculation of the Error Trend

We use an exponential window for calculation of the error trend from the sample errors as follows

$$E_{n+1} = \lambda\, E_n + (1-\lambda)\, |e_n|^2\,, \tag{4.34}$$

where λ is the forgetting factor ($0 \ll \lambda < 1$). We set the λ to a value that the effect of each error sample is decayed to one percent over the observation window, i.e.,

$$\lambda^{N_{\text{win}}} = 0.01. \tag{4.35}$$

4.5 Implementations and Numerical Results

Table 4.2 shows the simulation parameters. We use a wide-sense stationary (WSS) version of the Jakes fading [27] (which uses 14 low-frequency sinusoids) to examine the performance of the underlying algorithms. The Jakes fading is only valid for a rich scattering environment. Furthermore, because the Jakes fading is stationary, it can not model the changes in the scattering environment. To test the algorithms in a more realistic setting, we use a Ray-Tracing (RT) simulation environment as explained in [68]. The mobile is randomly moving vertically and horizontally in the scattering area, comprising of three buildings, and experiences different combinations of signal rays. At each point of the mobile path, it undergoes a different doppler frequency and a different signal power for each ray it receives. The generated fading, called "RT fading", can closely resemble the channel in a real mobile environment, and is used to examine the performance of the algorithms as well. The following two sections show the details of the implementation for LP and KF algorithms in our simulations.

4.5.1 Our Implementation of LP Algorithm

L1: Start

- Set $n = 0$

L2: Estimate the LP coefficients

- Estimate $\mathbf{a}_n$ from the Yule-Walker equations
- Calculate $\mathbf{a}_n^{(D)}$ from (4.15)

- Set $n_{\text{Acq}} = n$

L3: Set $n = n + 1$

L4: Linear Prediction

- Calculate $\hat{h}_{n+D|n}$ by (4.11)

L5: Acquisition time?

- If $n - n_{\text{Acq}} = T_{\text{AR}}$, then Goto L2

L6: Tracking the LP coefficients

- Calculate $\mathbf{a}_{n+1}$ by (4.16)
- Calculate $\mathbf{a}_{n+1}^{(D)}$ from (4.15)

L7: Goto L3

4.5.2 Our Implementation of KF Algorithm

L1: Start

- Set $n = 0$

L2: Model Acquisition

- Estimate $\omega_n(k)$'s and $\alpha_n(k)$'s using FFT
- Calculate $\mathbf{A}_n$ by (4.20)
- Set $n_{\text{Acq}} = n$

L3: Set $n = n + 1$

L4: Kalman filter

- Calculate $\mathbf{x}_{n|n}$ from (4.22)-(4.26)

L5: Predict the state vector

- Calculate (4.32)
- Calculate $\hat{\mathbf{x}}_{n+D|n}$ by (4.31)

L6: Error check

- Calculate E_{n+1} by (4.34)
- If $E_{n+1} \geq E_{\text{Thr}}$ and $n - n_{\text{Acq}} \geq T_{\text{Acq}}$, then Goto L2

L7: Tracking the Doppler frequencies

- Calculate (4.29)
- Calculate the sample error by (4.28)
- Calculate $\omega_{n+1}(k)$'s by (4.27)

L8: Goto L3

4.5.3 Simulation Results

To demonstrate how different parts of the proposed KF algorithm works, we show the results for a sample of RT fading at the mobile speed of $V = 25$ kmph in Figs. 4.4 - 4.6 as follows. Fig. 4.4 and Fig. 4.5 show the doppler frequencies $\omega_n(k)$'s and the magnitudes of the complex amplitudes $\alpha_n(k)$'s, respectively, and Fig. 4.6 depicts the trajectories of $|e_n|^2$ and E_n. For the RT fading sample used in this case, the fading

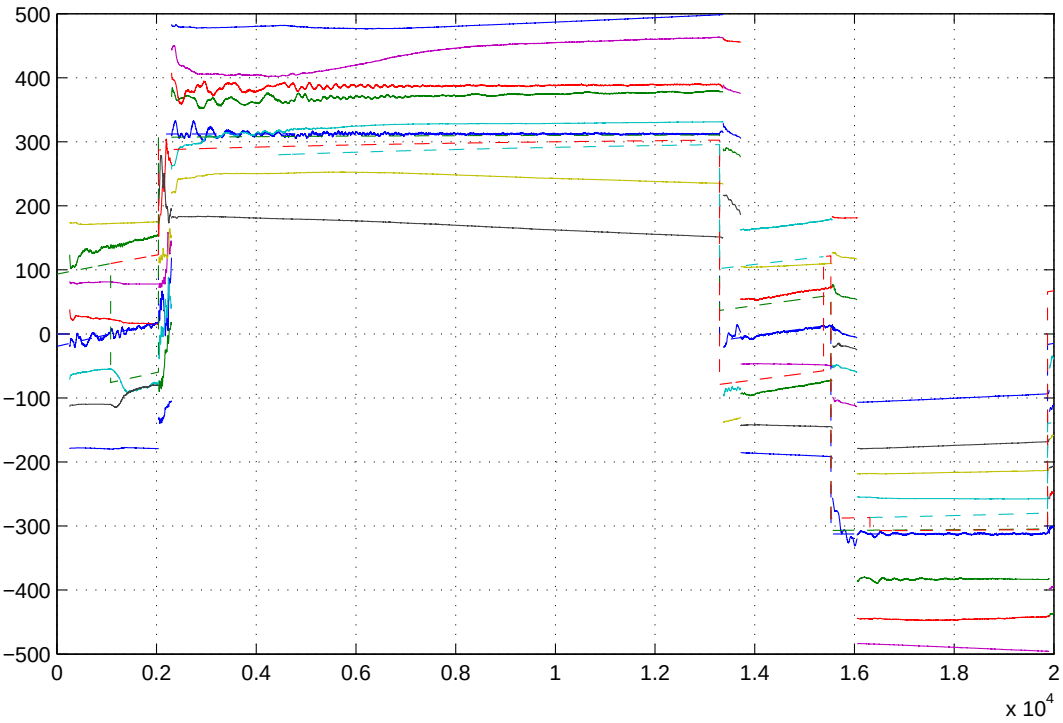

Figure 4.4: Estimation and tracking of the doppler frequencies

environment changes around the time samples of 0.2,1.35,1.55 and 2.0×10^4, corresponding to the times of change in the mobile direction. As explained before, when the scattering environment significantly changes, the algorithm detects the change through the error calculations and enters the acquisition mode. Consequently, the frequency unit, and then the Kalman filter converge to the parameters of the new model. This switch between the acquisition and tracking is clearly observable in the plots at the aforementioned times.

The two prediction algorithms (LP and KF) are compared here, with respect to the average MSE versus the prediction depth. The results are reported for various linear orders N_{AR}, and various scattering orders N_{ray}, respectively (N_{ray} is an approximation of N_{sc} in (4.18)). Fig. 4.7 shows the results for the Jakes fading for the mobile speeds

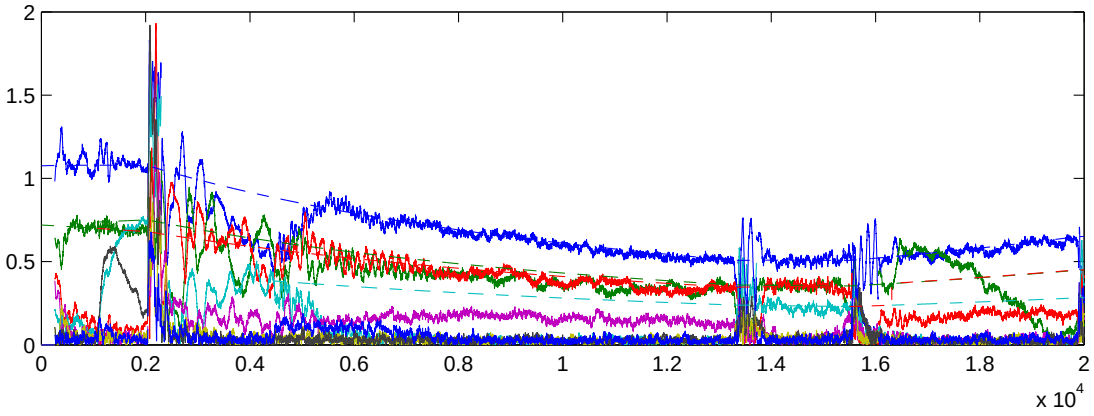

Figure 4.5: Kalman tracking of the amplitudes

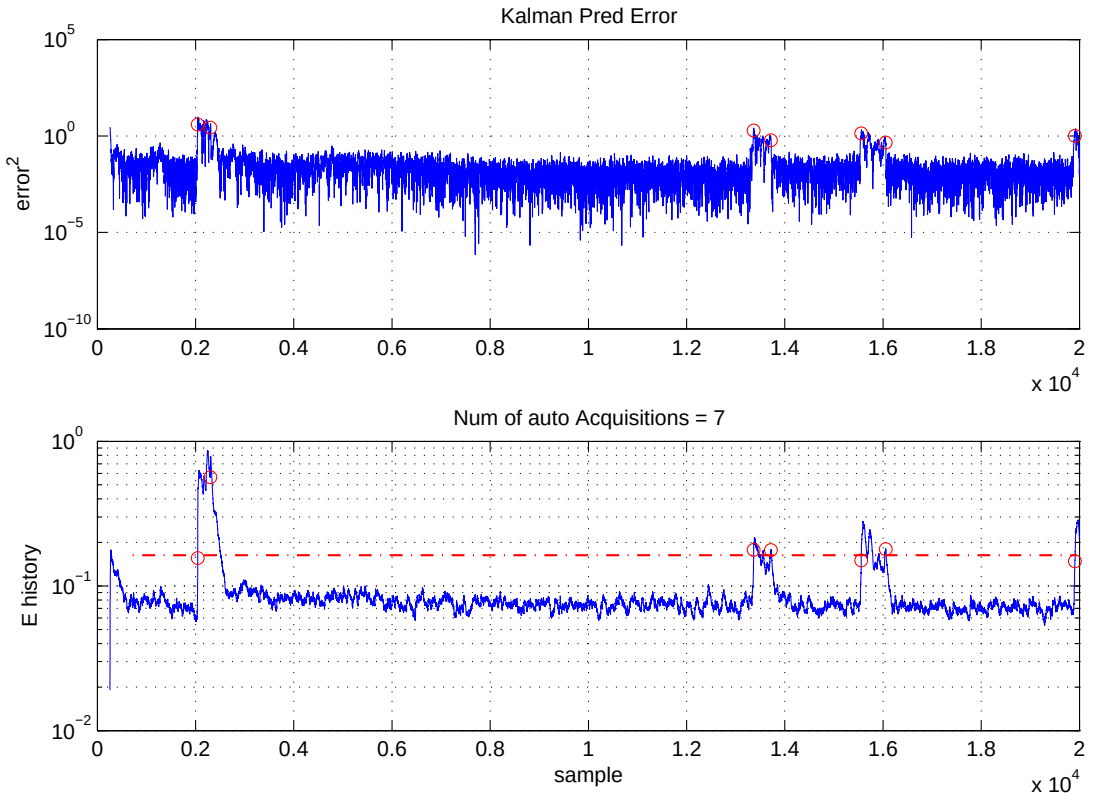

Figure 4.6: Error history for the Kalman filter

f_c	2.15 GHz
f_s	1500 Hz
SNR_z	10 dB

Table 4.2: Simulation parameters

of $V = 25$ and $V = 100$ kmph. It is observed that KF significantly outperforms LP if N_{ray} is large enough (here, for $N_{\mathrm{ray}} \geq 8$), while LP fails at high prediction depths regardless of the linear order N_{AR}.

Fig. 4.8 shows the results for RT fading for $V = 25$ and $V = 100$ kmph. It is observed that KF always outperform LP. For a linear predictor, the MSE is directly related to the correlation properties of the fading, i.e., a lower correlation results in a higher MSE. The fading correlation is not monotonic, therefore the MSE versus D plot may not be increasing at high mobile speeds as observed in Fig. 4.8 for $V = 100$ kmph. It is also observed that increasing N_{ray} does not always improve the performance. In conclusion, the simulations show that the proposed prediction algorithm can perform very well in realistic mobile environments, and it significantly outperforms the adaptive linear algorithm.

4.6 Conclusion

In this chapter, we have proposed a new method for prediction of fading channels. The doppler frequencies are estimated and updated by an acquisition-tracking method, and the amplitudes are updated by a Kalman filter. Because of its self-recovering nature, the algorithm is robust to the uncertainties such as the changes of the scattering environment, and the accuracy of the channel estimates (or observation SNR). The proposed algorithm has a reasonable complexity. Most of the existing algorithms have

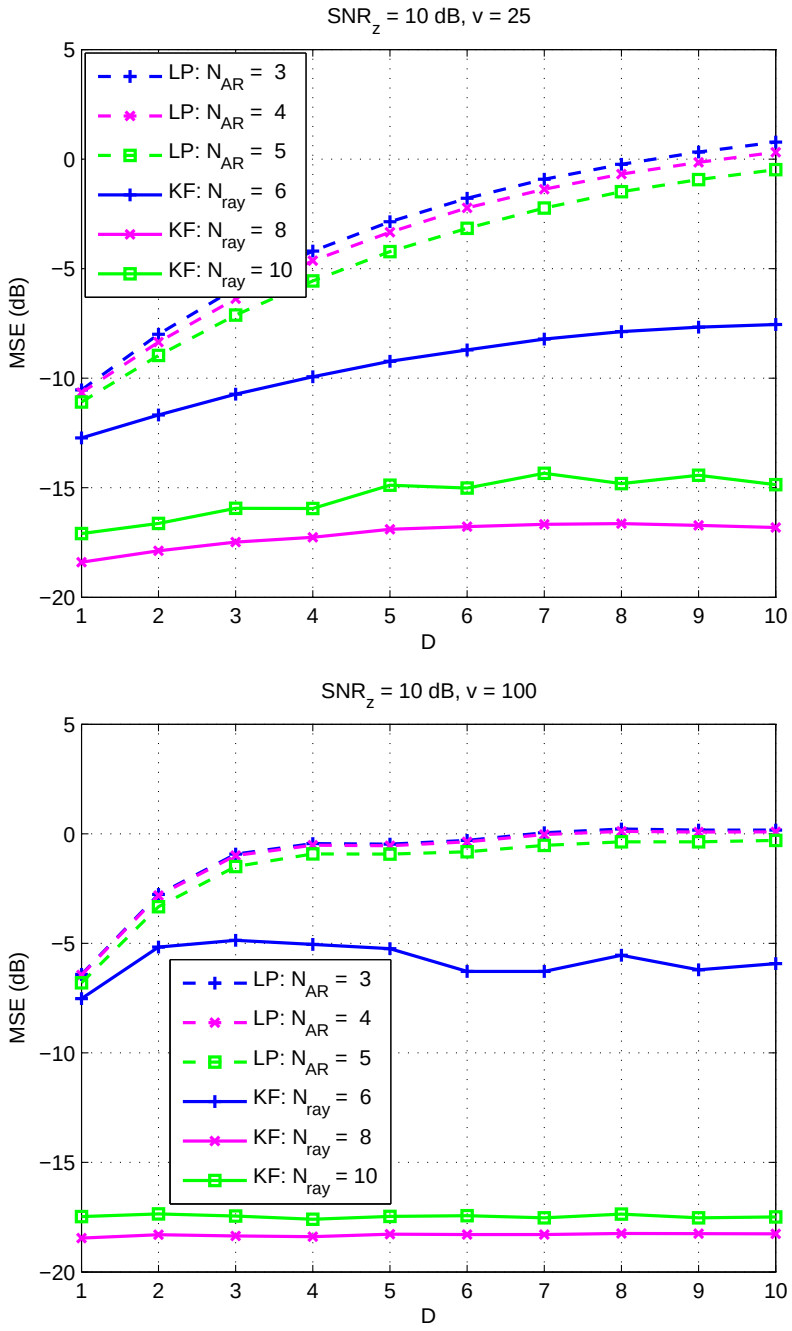

Figure 4.7: Comparison of MSE versus prediction depth for the Jakes fading at $V = 25$ and $V = 100$

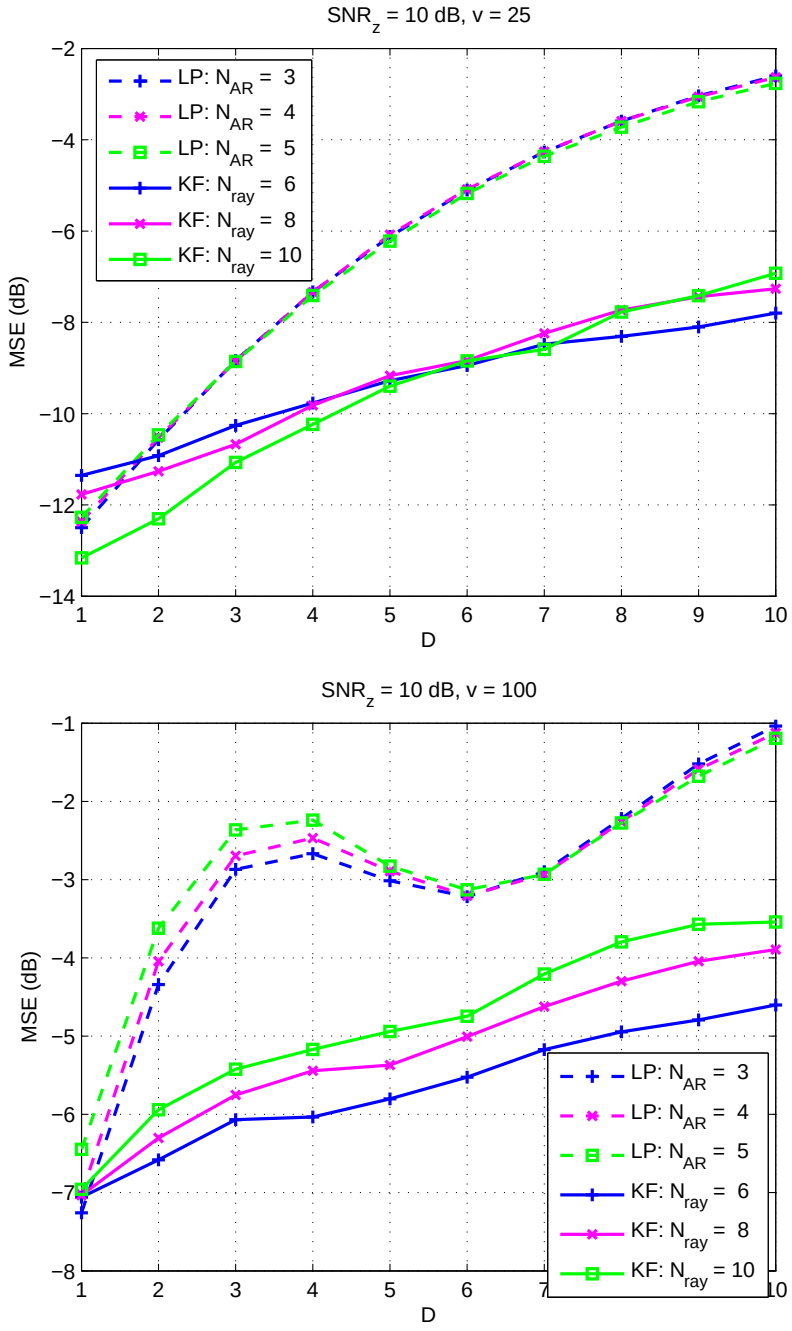

Figure 4.8: Comparison of MSE versus prediction depth for (non-stationary) RT fading at $V = 25$ and $V = 100$

a window-based structure requiring frequent high-complexity computations, while the proposed method has a sample-by-sample structure resulting in a steady flow of low-complexity calculations. The simulation results show the significant advantage of the algorithm over the conventional linear method, especially at high mobile speeds, and low observation SNR's.

Chapter 5

Conclusion and Future Work

This dissertation considers the problem of the efficient use of the channel state information in wireless and mobile communication systems. Considering the real conditions in such systems, various practical solutions are sought using the theoretical methods.

The closed-loop transmit diversity, which uses a combination of transmit diversity and channel feedback, is recognized as a promising approach to achieve high data rates in mobile communications. In the existing networks, however, the performance of the closed-loop scheme is limited, which is the result of the rate limit, error, and delay in the feedback channel, and also the non-optimum weight reconstruction algorithms.

In Chapter 2, we propose an approach to improve the performance of a closed-loop system in the presence of feedback error, without changing the existing structure (of the standard). We introduce a number of algorithms, using MAP and MMSE approaches, to improve the performance of mode 1 of 3GPP. It has been shown that our algorithms can provide significant gains over the conventional approach at all mobile speeds. The performance of our algorithms, which do not need any preamble, are usually good enough such that an Antenna Weight-Verification (AV) algorithm

is no longer required. Though, an AV could be used along with our algorithms for further improvement. Moreover, our proposed algorithms are implemented mostly at the base station, as opposed to AV which increases the complexity of the mobile unit.

Chapter 3 also considers the issue of feedback delay. We propose two approaches to improve the performance. One is based on using a channel predictor at the receiver to compensate for the delay, and using the method proposed in Chapter 2 to compensate for the feedback error. Another approach deals with both feedback error and delay in a unified reconstruction algorithm. Furthermore, we address the problem of the decoding mismatch at the receiver by proposing a Blind Antenna Verification (BAV) algorithm, which can substitute for the conventional AV process without the need for any training data. It is shown in that using the optimal reconstruction at the transmitter and the BAV algorithm (at the receiver) is a jointly optimal approach to achieve both the beamforming goal and the AV goal. A number of algorithms are introduced, and it is demonstrated that the proposed algorithms outperform the conventional methods at all mobile speeds, regardless of the quality of channel estimation. The structure of the proposed methods is suitable for the use in practical mobile radio systems, and particularly can be considered as a contribution to the 3GPP standard. Of course the proposed approaches in Chapter 2 and 3 could be used for the enhancement of any MIMO closed-loop communication system which uses quantized channel feedback.

Chapter 4 addresses the problems of modeling and prediction of mobile fading channels. First, a multi-step predictor is presented for a (linear) AR model, and a tracking algorithm for coefficients of the multi-step linear predictor is proposed. In the next parts, we propose a new method for prediction of fading channels, based

on a proposed state-space representation of the sum-sinusoidal model. The doppler frequencies are estimated and updated by an acquisition-tracking method, and the amplitudes are updated by a Kalman filter. Furthermore, a progressive prediction method is used for the multi-step prediction of the state vector. The algorithm is robust to the uncertainties such as the changes of the scattering environment and the accuracy of the channel estimates, and has a reasonable complexity. The simulations compare the two fading prediction methods, and show the significant advantage of the new method for both stationary and non-stationary fading. This performance advantage is larger at higher mobile speeds, and for longer predictions.

5.1 Future Work

The research presented in this dissertation may be continued in several directions. A number of the these continuations are described in the following.

5.1.1 MIMO Channel Modeling and Prediction

Based on Singular Value Decomposition, the MIMO channel can be split into independent sub-channels which allows efficient decoding of the transmitted data signal. Givens decomposition [75] can be utilized to convert the channel unitary matrix to a number of scalar parameters (of two different types) which are used in the subsequent processing. By dealing with the scalar parameters, the reconstruction of the unitary matrix can be analyzed using the feedback information.

For the prediction of the scalar parameters, proper models for the two parameter types are needed to be found. This modeling has not been done before, and is not analytically straightforward. Using an statistical approach, some models and the corresponding predictors can be developed. The modeling efficiency may be improved by inspecting other linear and nonlinear methods as well. This approach can be extended to the OFDM channels which are being used in the new generation of mobile radio systems. The research work suggested in this section is already completed in part [76].

MIMO Channel Quantization

The proposed method for modeling a MIMO channel is suitable for development of MIMO precoding schemes, adaptive transmission methods, etc., where the channel

state information is partially required at the transmitter. In this direction, an efficient quantization method [77, 78] is needed for the equivalent scalar parameters. To combat the feedback delay and feedback error in these systems, the methods introduced in chapter 2 and 3 can be similarly applied. Furthermore, the optimal resource allocation (e.g., number of bits for each parameter) at different conditions is open for research.

5.1.2 Precoding for MIMO Channels

The problem of adaptive transmission and precoding for MIMO channels has been widely studied in the literature. However, the suggested designs are not usually optimal in practice, because they do not consider the error, delay or even the quantization error in the available feedback information. Furthermore, the optimal decoding is such systems is rarely addressed. Using the techniques introduced in this dissertation, new MIMO precoding schemes can be designed for practical conditions.

5.1.3 New Generation of Closed-loop Schemes

We proposed a joint beamforming and decoding scheme using imperfect feedback, which is compatible with the 3GPP standard, in chapter 3. Dropping the assumption of the compatibility with the 3GPP standard, new closed-loop schemes can be developed for the next generation of mobile systems. Design of new quantization schemes by considering the feedback imperfections is a vast and challenging area of research.

Appendix A

Calculation of the Number of States (or the Codebook Size)

Consider the framing structure of mode 1 of 3GPP, depicted in Fig. 2.6. In the figure, each slot shows the quantizer used according to Section 2.3. At time slot n, the current state is composed of γ symbols, from the starting slot number $n_{win} = n - \gamma + 1$ to the slot number n, which is shown by dashed sliding windows. The windows shown in the figure correspond to the case $\gamma = 3$, but our discussion is for any value of $0 < \gamma < 15$. For a given window, specified by n_{win}, there are 2^γ possible states. Depending on the window position, there are two cases:

Case 1: For $n_{win} = 0, 1, \cdots, 15 - \gamma$, the window is within one frame, and the symbols are selected from Q_0 and Q_1, consecutively. Therefore, for all of the odd n_{win}'s, the sequence of possible subsets are the same. This is also the case for all even n_{win}'s. Hence, there are two possible sequences of subsets for this range of n_{win}, resulting in $2 \times 2^\gamma$ different states.

Case 2: For $n_{win} = 16 - \gamma, \cdots, 14$, the window is in two neighboring frames. The symbols are also selected from Q_0 and Q_1 consecutively, except for the slots at the boundary of the two frames where symbols are selected from two consecutive Q_0. Therefore, for each n_{win} in the range, the sequences of possible subsets are unique, and different from case 1. Hence, there are $14-(16-\gamma)+1 = \gamma-1$ possible sequences of subsets for this range of n_{win}, resulting in $(\gamma - 1)\, 2^{\gamma}$ different states.

Adding up the possible states of the two cases, it leads to $(\gamma+1)\, 2^{\gamma}$ possible states for the structure of mode 1 of 3GPP. Note that a similar deduction could be done to calculate the codebook size by replacing γ with μ, which results in $(\mu + 1)\, 2^{\mu}$.

Appendix B

Proof of Lemma 1

The variable $\hat{w}^{normal} = \alpha e^{j\hat{\phi}}$ should be estimated using the random variable $w = \beta e^{j\phi}$, where α and β are real positive constants. In the MMSE sense, it turns out to minimizing the following criterion

$$
\begin{aligned}
& E\left[\left|w - \hat{w}^{normal}\right|^2\right] && \text{(B.1)} \\
= \; & E\left[\left|\beta e^{j\phi} - \alpha e^{j\hat{\phi}}\right|^2\right] && \text{(B.2)} \\
= \; & \alpha^2 + \beta^2 - 2\alpha\beta\, E\left[\cos(\phi - \hat{\phi})\right] && \text{(B.3)}
\end{aligned}
$$

or maximizing

$$
\begin{aligned}
& E\left[\cos(\phi - \hat{\phi})\right] && \text{(B.4)} \\
= \; & E\left[\cos\phi\cos\hat{\phi} + \sin\phi\sin\hat{\phi}\right] && \text{(B.5)} \\
= \; & E[\cos\phi]\cos\hat{\phi} + E[\sin\phi]\sin\hat{\phi} && \text{(B.6)}
\end{aligned}
$$

which results in

$$
\tan\hat{\phi} = \frac{E[\sin\phi]}{E[\cos\phi]}, \qquad \text{(B.7)}
$$

where

$$\begin{cases} E[\cos\phi] \geq 0 & \Rightarrow \ -\frac{\pi}{2} < \hat{\phi} \leq \frac{\pi}{2} \\ E[\cos\phi] < 0 & \Rightarrow \quad \frac{\pi}{2} < \hat{\phi} \leq 3\frac{\pi}{2} \end{cases} \tag{B.8}$$

Finding the phase information of $\hat{w}^{normal}$, i.e., $e^{j\hat{\phi}} = \cos\hat{\phi} + j\,\sin\hat{\phi}$, from (B.7), it is easy to show that in both cases of (B.8),

$$e^{j\hat{\phi}} = \frac{E[e^{j\phi}]}{|E[e^{j\phi}]|}. \tag{B.9}$$

Therefore,

$$\hat{w}^{normal} = \alpha\, e^{j\hat{\phi}} = \alpha\, \frac{E[e^{j\phi}]}{|E[e^{j\phi}]|} = \alpha\, \frac{E[w]}{|E[w]|}. \tag{B.10}$$

Appendix C

Proof of Lemma 2

Using the data processing theorem, we know that

$$\underline{\mathbf{w}}_n \leftrightarrow \underline{I}_{n-d} \leftrightarrow \underline{J}_{n-d} \tag{C.1}$$

forms a Markov chain, because the feedback sequence $\underline{I}_{n-d}$ is calculated from the weight sequence $\underline{\mathbf{w}}_n$ at the receiver, and $\underline{J}_{n-d}$, which is received at the transmitter after passing through the feedback channel, is an (stochastically) impaired version of $\underline{I}_{n-d}$. Therefore, for the conditional PDF's, it can be written

$$f\left(\underline{\mathbf{w}}_n|\underline{I}_{n-d}, \underline{J}_{n-d}\right) = f\left(\underline{\mathbf{w}}_n|\underline{I}_{n-d}\right). \tag{C.2}$$

Now, the following integration of both sides

$$\int_{\underline{\mathbf{w}}_{n-1}} \cdots \int f\left(\underline{\mathbf{w}}_n|\underline{I}_{n-d}, \underline{J}_{n-d}\right) d\underline{\mathbf{w}}_{n-1} = \int_{\underline{\mathbf{w}}_{n-1}} \cdots \int f\left(\underline{\mathbf{w}}_n|\underline{I}_{n-d}\right) d\underline{\mathbf{w}}_{n-1}, \tag{C.3}$$

results in

$$f\left(\mathbf{w}_n|\underline{I}_{n-d}, \underline{J}_{n-d}\right) = f\left(\mathbf{w}_n|\underline{I}_{n-d}\right), \tag{C.4}$$

meaning that

$$\mathbf{w}_n \leftrightarrow \underline{I}_{n-d} \leftrightarrow \underline{J}_{n-d} \tag{C.5}$$

is a Markov chain.

Appendix D

Proof of Lemma 3

As a property of a Markov chain,

$$f(x|y,z) = f(x|y), \tag{D.1}$$

where $f(\cdot)$ is the PDF of the respective random variable. Hence,

$$\begin{aligned}
E_Y\left[E_X[X|Y]|Z\right] = & && \text{(D.2)}\\
& \int \left(\int x f(x|y) dx \right) f(y|z) dy && \text{(D.3)}\\
= & \int \int x f(x|y) f(y|z) dx dy && \text{(D.4)}\\
= & \int \int x f(x|y,z) f(y|z) dx dy && \text{(D.5)}\\
= & \int \int x f(x,y|z) dx dy && \text{(D.6)}\\
= & \int x f(x|z) dx && \text{(D.7)}\\
= & E_X[X|Z]. && \text{(D.8)}
\end{aligned}$$

Appendix E

Derivation of the State Probabilities for Receiver

The probability values of $P(S_n|\underline{I}_{n-d})$ are needed at the receiver for the calculation of the weight. We can write

$$P(S_n|\underline{I}_{n-d}) = P(S_n|\underline{S}_{n-d}) \tag{E.1}$$

$$= \quad P(S_n|S_{n-d}), \tag{E.2}$$

where $P(S_n|S_{n-d})$ is the d-step transition probability which is calculated once as follows

$$P(S_n|S_{n-d}) = P(S_n|\underline{S}_{n-d}) \tag{E.3}$$

$$= \sum_{\underline{S}_{n-1}^{n-d-1}} \cdots \sum P(S_n|S_{n-1}) \cdot$$

$$P(S_{n-1}|S_{n-2}) \cdots P(S_{n-d-1}|S_{n-d}). \tag{E.4}$$

Appendix F

Multi-step Tracking of the AR Coefficients

Assume that δ_n is the increment vector

$$\mathbf{a}_{n+1} = \mathbf{a}_n + \delta_n. \tag{F.1}$$

From (F.1) and (4.7), we may write

$$\mathbf{B}_{n+1} = \mathbf{B}_n + \Delta_n \tag{F.2}$$

where

$$\Delta_n = \begin{pmatrix} \delta_n^T \\ \mathbf{0}_{(\mathbf{N}_{\mathrm{AR}}-\mathbf{1})\times\mathbf{N}_{\mathrm{AR}}} \end{pmatrix} \tag{F.3}$$

For the D-step predictor, we write

$$\mathbf{B}_{n+1}^D = \mathbf{B}_n^D + \Delta_n^{(D)}. \tag{F.4}$$

The structure of $\Delta_n^{(D)}$ may not exactly be as shown in (F.3), however, we show the first row of $\Delta_n^{(D)}$ as $\delta_n^{(D)}$.

Assuming a sufficiently large sampling frequency, $\mathbf{a}_n$ is slowly changing with the time index n, and δ_n has a small norm. Therefore,

$$\mathbf{B}_{n+1}^D = (\mathbf{B}_n + \Delta_n)^D \tag{F.5}$$

$$\cong \mathbf{B}_n^D + \sum_{i=1}^{D} \mathbf{B}_n^{i-1} \Delta_n \mathbf{B}_n^{D-i} \tag{F.6}$$

where (F.6) is approximated by neglecting the terms in which Δ_n has a power larger than one. Hence,

$$\Delta_n^{(D)} \cong \sum_{i=1}^{D} \mathbf{B}_n^{i-1} \Delta_n \mathbf{B}_n^{D-i} \tag{F.7}$$

From (F.4) we may write

$$\mathbf{a}_{n+1}^{(D)} = \mathbf{a}_n^{(D)} + \delta_n^{(D)}, \tag{F.8}$$

which corresponds to the operation of the first rows of the matrices. Now, $\delta_n^{(D)}$ can be calculated using δ_n as follows,

$$\delta_n \rightarrow \Delta_n \rightarrow \Delta_n^{(D)} \rightarrow \delta_n^{(D)}. \tag{F.9}$$

It is observed from (F.7) that each element of $\Delta_n^{(D)}$ is a linear combination of the elements of Δ_n (or equivalently δ_n). Therefore, each element of $\delta_n^{(D)}$ is a linear combination of δ_n and so we can write

$$\delta_n^{(D)} = \mathbf{G}_n^{(D)} \delta_n \tag{F.10}$$

where matrix $\mathbf{G}_n^{(D)}$ represents the linear combinations. Matrix $\mathbf{G}_n^{(D)}$ is a function of $\mathbf{B}_n$ or equivalently a function of the elements of $\mathbf{a}_n$. As an example, $\mathbf{G}_n^{(D)}$ for $D = 1, 2, 3$ are shown in (F.11)-(F.13), when $N_{\text{AR}} = 3$:

$$\mathbf{G}_n^{(1)} = \begin{pmatrix} 1 & 0 & 0 \\ 0 & 1 & 0 \\ 0 & 0 & 1 \end{pmatrix}, \tag{F.11}$$

$$\mathbf{G}_n^{(2)} = \begin{pmatrix} 2\,a_n(1) & 1 & 0 \\ a_n(2) & a_n(1) & 1 \\ a_n(3) & 0 & a_n(1) \end{pmatrix}, \tag{F.12}$$

$$\mathbf{G}_n^{(3)} = \begin{pmatrix} 3\,a_n(1)^2 + 2\,a_n(2) & 2\,a_n(1) & 1 \\ 2\,a_n(1)\,a_n(2) + a_n(3) & 2\,a_n(2) + a_n(1)^2 & a_n(1) \\ 2\,a_n(1)\,a_n(3) & a_n(3) & a_n(1)^2 + a_n(2) \end{pmatrix} \cdots \tag{F.13}$$

It is observed that the analytical form of $\mathbf{G}_n^{(D)}$ is more complicated for a larger D. For most applications $\mathbf{a}_n$ is slowly changing, hence $\mathbf{G}_n^{(D)}$ may be recalculated only in the acquisition mode. This approximation can be further simplified if $\mathbf{G}_n^{(D)}$ is calculated for a fixed typical channel. For example, for the channel $\mathbf{a} = [1,\, 0,\, \cdots,\, 0]^T$, $\mathbf{G}_n^{(D)}$ has a simple form; when $N_{\mathrm{AR}} = 3$,

$$\mathbf{G}_n^{(D)} \approx \begin{pmatrix} D & D-1 & D-2 \\ 0 & 1 & 1 \\ 0 & 0 & 1 \end{pmatrix}. \tag{F.14}$$

Our simulations show that the performance does not change significantly with this approximation in a wide range of mobile speed and D.

Appendix G

Extension of the Proposed Fading Model

We provided a state-space model for a single-path SISO channel in Section 4.3.2. To extend the model to MIMO and/or multipath channels, the same approach can be used. Assume there is a total of N_{ch} different channels, where each one uses N_{ray} sinusoids. Furthermore, assume that each channel has N_{mp} resolvable multipath. The model can be shown as follows,

$$\begin{cases} \mathbf{X}_n = \mathbf{A}_n \, \mathbf{X}_{n-1} + \mathbf{Q}_n \\ \mathbf{Z}_n = \mathbf{M}_n \, \mathbf{X}_n + \mathbf{V}_n \end{cases} \tag{G.1}$$

Each variable plays the same role as in (4.19). $\mathbf{X}_n$ is a $N_{\text{ch}} N_{\text{ray}} \times N_{\text{mp}}$ matrix which is constructed by stacking the state vectors of different channels and different multipath

components as follows

$$\mathbf{X}_n = \begin{pmatrix} \mathbf{x}_n(1,1) & \mathbf{x}_n(1,2) & \cdots & \mathbf{x}_n(1,N_{\mathrm{mp}}) \\ \mathbf{x}_n(2,1) & \mathbf{x}_n(2,2) & \cdots & \mathbf{x}_n(2,N_{\mathrm{mp}}) \\ \vdots & \vdots & & \vdots \\ \mathbf{x}_n(N_{\mathrm{ch}},1) & \mathbf{x}_n(N_{\mathrm{ch}},2) & \cdots & \mathbf{x}_n(N_{\mathrm{ch}},N_{\mathrm{mp}}) \end{pmatrix} \tag{G.2}$$

where $\mathbf{x}_n(i,j)$ is the $N_{\mathrm{ray}} \times 1$ state vector of the j-th multipath of the i-th channel. $\mathbf{A}_n$ is a square matrix with $N_{\mathrm{ch}}N_{\mathrm{ray}}$ diagonal elements containing the doppler frequencies, $\mathbf{Z}_n$ and $\mathbf{V}_n$ are $N_{\mathrm{ch}} \times N_{\mathrm{mp}}$ matrices which contain the observation and the observation noise for each channel at time n, respectively. $\mathbf{M}_n$ is a $N_{\mathrm{ch}} \times N_{\mathrm{ch}}N_{\mathrm{ray}}$ matrix as depicted in the following,

$$\mathbf{M}_n = \begin{pmatrix} \mathbf{1} & & & \\ & \mathbf{1} & & \\ & & \ddots & \\ & & & \mathbf{1} \end{pmatrix} \tag{G.3}$$

containing N_{ch} "$\mathbf{1}$"-vectors defined as

$$\mathbf{1} = [1,\ 1,\ \cdots,\ 1]_{1 \times N_{\mathrm{ray}}} \tag{G.4}$$

Appendix H

Tracking Algorithm for the Doppler Frequencies

Considering the definition of $\mathbf{x}_n$ in (4.19), from (4.18) it can be written

$$\hat{h}_n = \sum_{k=1}^{N_{\text{sc}}} x_{n-1}(k)\, e^{j\omega_n(k)T_s}, \tag{H.1}$$

as the phase-shifts of the sinusoidal terms up to the time $n-1$ are absorbed in $x_{n-1}(k)$.

Assume the cost function

$$C_n = E\left[\left|h_n - \hat{h}_n\right|^2\right] \tag{H.2}$$

$$= E\left[|e_n|^2\right], \tag{H.3}$$

where

$$e_n = h_n - \hat{h}_n. \tag{H.4}$$

Hence, a gradient-based tracking algorithm can be implemented as

$$w_{n+1}(k) = w_n(k) - \mu_0 \frac{\partial C_n}{\partial w_n(k)}. \tag{H.5}$$

To derive the LMS algorithm, we can write

$$\begin{aligned}
\frac{\partial C_n}{\partial w_n(k)} &\approx \frac{\partial \left|e_n\right|^2}{\partial w_n(k)} && \text{(H.6)}\\
&= \frac{\partial (e_n^H\, e_n)}{\partial w_n(k)} && \text{(H.7)}\\
&= 2\,\Re\left[(-j\,T_s\,x_{n-1}(k)\,e^{j\omega_n(k)T_s})^H\,e_n\right] && \text{(H.8)}\\
&= 2\,\Re\left[(-j\,T_s\,x_n(k))^H\,e_n\right] && \text{(H.9)}\\
&= 2\,\Re\left[j\,T_s\,x_n^H(k)\,e_n\right] && \text{(H.10)}\\
&= -2\,T_s\,\Im\left[x_n^H(k)\,e_n\right] && \text{(H.11)}
\end{aligned}$$

where $\Re$ and $\Im$ are the real and imaginary operators, respectively. Equation (H.6) is obtained by replacing the $E[\cdot]$ of the error term in (H.3) with the instantaneous value. Now, we can write the LMS algorithm as follows

$$w_{n+1}(k) = w_n(k) + \mu\,\Im\left[x_n^H(k)\,e_n\right], \qquad \text{(H.12)}$$

where $\mu = 2\,T_s\,\mu_0$ is the step size.

Appendix I

Multi-step Prediction of the State Vector

Assume the state-space model shown in (4.19). The state at the time $n+D$ could be written as

$$\begin{aligned} \mathbf{x}_{n+D} &= \mathbf{A}_{n+D}\,\mathbf{x}_{n+D-1} + \mathbf{q}_{n+D} && \text{(I.1)} \\ &= \mathbf{A}_{n+D}\,\left(\mathbf{A}_{n+D-1}\,\mathbf{x}_{n+D-2} + \mathbf{q}_{n+D-1}\right) + \mathbf{q}_{n+D} && \text{(I.2)} \\ &= \mathbf{A}_{n+D}\mathbf{A}_{n+D-1}\mathbf{x}_{n+D-2} + \mathbf{A}_{n+D}\mathbf{q}_{n+D-1} + \mathbf{q}_{n+D}. && \text{(I.3)} \end{aligned}$$

Continuing this calculation results in

$$\begin{aligned} \mathbf{x}_{n+D} &= \mathbf{A}_{n+D}\mathbf{A}_{n+D-1}\cdots\mathbf{A}_{n+1}\mathbf{x}_n + \\ &\quad \mathbf{A}_{n+D}\mathbf{A}_{n+D-1}\cdots\mathbf{A}_{n+2}\mathbf{q}_{n+1} + \cdots \\ &\quad + \mathbf{A}_{n+D}\mathbf{q}_{n+D-1} + \mathbf{q}_{n+D} && \text{(I.4)} \end{aligned}$$

Hence, for prediction of $\mathbf{x}_{n+D}$ given the available observation data up to the time n, from (I.4), we have

$$\begin{aligned}
\hat{\mathbf{x}}_{n+D|n} &= E\left[\mathbf{x}_{n+D}|\underline{z}_n\right] && \text{(I.5)}\\
&= \mathbf{A}_{n+D}\mathbf{A}_{n+D-1}\cdots\mathbf{A}_{n+1}E\left[\mathbf{x}_n|\underline{z}_n\right] + \\
&\quad 0+\cdots+0+0 && \text{(I.6)}\\
&= \mathbf{A}_{n+D}\mathbf{A}_{n+D-1}\cdots\mathbf{A}_{n+1}\,\mathbf{x}_{n|n} && \text{(I.7)}
\end{aligned}$$

using the fact that $E[\mathbf{q}_i|\underline{z}_n] = 0$, $i > n$.

Finally, the fading sample at the time $n+D$ can be predicted as

$$\begin{aligned}
\hat{h}_{n+D|n} &= E\left[h_{n+D}|\underline{z}_n\right] && \text{(I.8)}\\
&= E\left[\mathbf{m}_{n+D}\,\mathbf{x}_{n+D} + v_{n+D}|\underline{z}_n\right] && \text{(I.9)}\\
&= \mathbf{m}_{n+D}\,\hat{\mathbf{x}}_{n+D|n} && \text{(I.10)}\\
&= \mathbf{m}_{n+D}\,\mathbf{A}_{n+D}\mathbf{A}_{n+D-1}\cdots\mathbf{A}_{n+1}\,\mathbf{x}_{n|n}. && \text{(I.11)}
\end{aligned}$$

Appendix J

Tracking the Multi-step Transition Matrix

Consider the proposed state-space model described in Section 4.3.2. Implementing (I.11), it can be written

$$\mathbf{A}_{n+D}\cdots\mathbf{A}_{n+1} = diag\left[e^{j\{\omega_{n+D}(1)+\cdots+\omega_{n+1}(1)\}T_s},\ \cdots,\ e^{j\{\omega_{n+D}(N_{\text{ray}})+\cdots+\omega_{n+1}(N_{\text{ray}})\}T_s}\right] \quad \text{(J.1)}$$

The doppler frequencies are slowly changing. To track these changes, we assume a first order model and use linear extrapolation to write

$$\mathbf{w}_{n+d} \cong \mathbf{w}_n + d\,\delta\mathbf{w}_n, \quad d = 1, 2, \cdots, D. \quad \text{(J.2)}$$

where $\delta\mathbf{w}_n = \mathbf{w}_{n+1} - \mathbf{w}_n$. Consequently,

$$\begin{aligned}\mathbf{A}_{n+D}\cdots\mathbf{A}_{n+1} &= diag\left[e^{j\{D\,\omega_n(1)+(D+\cdots+2+1)\,\delta\omega_n(1)\}T_s},\right.\\ &\qquad \left.\cdots,\ e^{j\{D\,\omega_n(N_{\text{ray}})+(D+\cdots+2+1)\,\delta\omega_n(N_{\text{ray}})\}T_s}\right] \quad \text{(J.3)}\\ &= \mathbf{A}_n^D\ diag\left[e^{j\frac{D(D+1)}{2}\,\delta\mathbf{w}_n T_s}\right]. \quad \text{(J.4)}\end{aligned}$$

Bibliography

[1] 3GPP Technical Specification, "UMTS Physical Layer Procedures (FDD)," *ETSI TS 125 214 V6.0.0*, Dec. 2003.

[2] I. E. Teletar, "Capacity of Multi-antenna Gaussian Channels," *Technical Memorandum, Bell Laboratories, Lucent Technologies*, Oct. 1995.

[3] "The 3GPP website: `http://www.3gpp.org`."

[4] "The 3GPP2 website: `http://www.3gpp2.org`."

[5] 3GPP Technical Specification, "UMTS Physical Layer: General Description," *ETSI TS 125 201 V6.0.0*, Dec. 2003.

[6] R. T. Derryberry et al., "Transmit Diversity in 3G CDMA Systems," *IEEE Communications Magazine*, pp. 68–75, Apr. 2002.

[7] A. Heidari and A. K. Khandani, "Closed-Loop Transmit Diversity with Imperfect Feedback," *submitted to IEEE Transactions on Wireless Communications*, 2007.

[8] E. N. Onggosanusi et al., "Performance Analysis of Closed-Loop Transmit Diversity in the Presence of Feedback Delay," *IEEE Trans. on Communications*, pp. 1618–1630, Sep. 2001.

[9] J. Du, Y. Li, D. Gu, A. F. Molisch, J. Zhang, "Estimation of performance loss due to delay in channel feedback in MIMO systems," *IEEE Vehicular Technology Conference*, pp. 1619–1622, Sep. 2004.

[10] J. Hamalainen and R. Wichman, "Performance Analysis of Closed-Loop Transmit Diversity in the Presence of Feedback Errors," *International Symposium on Personal, Indoor and Mobile Radio Communications*, pp. 2297–2301, Sep. 2002.

[11] A. Heidari, F. Lahouti, and A. K. Khandani, "Improved Reconstruction of Channel State Information for Low-Rate Feedback Schemes," *IEEE Trans. on Vehicular Technology*, vol. 56, no. 5, pp. 2941–2953, Sep. 2007.

[12] ——, "Improved Reconstruction of Channel State Information in 3GPP," *Vehicular Technology Conference (VTC'F05), Dallas, Texas, USA*, Sep. 2005.

[13] A. Seeger and M. Sikora, "Antenna Weight Verification for Closed-Loop Transmit Diversity," *IEEE Global Telecommunications Conference (GLOBECOM)*, pp. 1124–1129, Dec. 2003.

[14] G. E. Oien, H. Holm, K. J. Hole, "Impact Of Channel Prediction On Adaptive Coded Modulation Performance In Rayleigh Fading," *IEEE Transactions on Vehicular Technology*, pp. 758 – 769, May 2004.

[15] A. Duel-Hallen and S. Hu, H. Hallen, "Long Range Prediction of Fading Signals: Enabling Adaptive Transmission for Mobile Radio Channels," *IEEE Signal Processing Magazine*, May 2000.

[16] A. Heidari, and A. K. Khandani, "Improved Closed-Loop Communication in the Presence of Feedback Delay and Error," *Conference on Information Sciences and Systems (CISS)*, pp. 289–294, Mar. 2006.

[17] W. C. Jakes, Ed., *Microwave Mobile Communications*. New York: IEEE Press, 1974.

[18] T. Eyceoz, A. Duel-Hallen, and H. Hallen, "Deterministic Channel Modeling and Long Range Prediction of Fast Fading Mobile Radio Channels," *IEEE Communications Letters*, Sep. 1998.

[19] T. S. Rappaport, *Wireless Communications: Principles and Practice.* Prentice-Hall, 1996.

[20] Vahid Tarokh, N. Seshadri, and A. R. Calderbank, "SpaceTime Codes for High Data Rate Wireless Communication: Performance Criterion and Code Construction," *IEEE Trans. on Information Theory*, pp. 744–765, Mar. 1998.

[21] S. M. Alamouti, "A Simple Transmitter Diversity Scheme for Wireless Communications," *IEEE Journal on Selected Areas in Communications*, pp. 1451–1458, Oct. 1998.

[22] E. Visotsky and U. Madhow, "Space-Time Precoding with Imperfect Feedback," *IEEE Trans. on Information Theory*, pp. 2632–2639, Sep. 2001.

[23] H. Gerlach, "SNR Loss due to Feedback Quantization and Errors in Closed Loop Transmit Diversity Systems," *The 13th IEEE International Symposium on Personal, Indoor and Mobile Radio Communications (PIMRC)*, pp. 2117–2120, Sep. 2002.

[24] J. Hamalainen and R. Wichman, "The Effect of Feedback Delay to the Closed-Loop Transmit Diversity in FDD WCDMA," *International Symposium on Personal, Indoor and Mobile Radio Communications*, pp. D–27–D–31, Oct. 2001.

[25] A. Hottinen and R. Wichman, "Transmit diversity using Filtered Feedback Weights in the FDD/WCDMA System," *Proceedings of Broadband Communications*, pp. 15–21, Feb. 2000.

[26] J. G. Proakis, *Digital Communications.* Mc-Graw Hill International Editions, 2001.

[27] M. F. Pop and C. Beauliu, "Limitations of Sum-of-Sinusoids Fading Channel Simulators," *IEEE Trans. on Communications*, pp. 699–708, Apr. 2001.

[28] A. Narula, M. J. Lopez, M. D. Trott, and G. W. Wornell, "Efficient Use of Side Information In Multiple-Antenna Data Transmission Over Fading Channels," *IEEE Journal on selected Areas in Communications*, pp. 1423–1436, Oct. 1998.

[29] B.A. Bjerke, Z. Zvonar, and J. G. Proakis, "Antenna Diversity Combining Schemes For WCDMA Systems In Fading Multipath Channels," *IEEE Trans. on Wireless Communications*, pp. 97–106, Jan. 2004.

[30] P. A. Dighe, R. K. Mallik, and S. S. Jamuar, "Analysis of Transmit-Receive Diversity in Rayleigh Fading," *IEEE Trans. on Communications*, pp. 694–703, Apr. 2003.

[31] A. Narula, M. D. Trott, and G. W. Wornell, "Performance Limits of Coded Diversity Methods for Transmitter Antenna Array," *IEEE Trans. on Information Theory*, pp. 2418–2433, Nov. 1999.

[32] D. J. Love, R. W. Heath, and T. Strohmer, "Grassmannian Beamforming for Multiple-Input Multiple-Output Wireless Systems," *IEEE Trans. on Information Theory*, pp. 2735–2747, Oct. 2003.

[33] K. C. Hwang and K. B. Lee, "Efficient Weight Vector Representation for Closed-Loop Transmit Diversity," *IEEE Trans. on Communications*, pp. 9–16, Jan. 2004.

[34] K. K. Mukkavilli, A. Sabharwal, E. Erkip, and B. Aazhang, "On Beamforming With Finite Rate Feedback In Multiple-Antenna Systems," *IEEE Trans. on Information Theory*, pp. 2562–2579, Oct. 2003.

[35] M. Edlund, M. Skoglund, and B. D. Rao, "On The Performance Of Closed-Loop Transmit Diversity With Non-Ideal Feedback," *IEEE International Conference on Communications (ICC)*, pp. 3190–3194, May 2003.

[36] Texas Instruments, "Modified Closed Loop Modes for WCDMA," *3GPP TSGR1 7(99)c86*, Aug. 1999.

[37] A. Seeger, M. Sikora, and W. Utschick, "Antenna Weight Verification for Closed-Loop Downlink Eigenbeamforming," *IEEE Global Telecommunications Conference (GLOBECOM)*, pp. 982–986, Nov. 2002.

[38] A. Serratore and E. Messina, "Analytical Evaluation And Performance Analysis Of Antenna Verification Algorithm In Closed Loop Antenna Diversity," *The 9th Asia-Pacific Conference on Communications (APCC)*, pp. 9–14, Sep. 2003.

[39] B. Raghothaman, R. T. Derryberry, and G. Mandyam, "Transmit Adaptive Array Without User-Specific Pilot For 3G CDMA," *IEEE International Conference on Acoustics, Speech, and Signal Processing (ICASSP)*, pp. 3009–3012, Jun. 2000.

[40] F. Lahouti and A. K. Khandani, "Efficient Source Decoding over Memoryless Noisy Channels using Higher Order Markov Models," *IEEE Trans. on Information Theory*, pp. 2103–2118, Sep. 2004.

[41] ——, "Reconstruction of Predictively Encoded Signals over Noisy Channels Using a Sequence MMSE Decoder," *IEEE Trans. on Communications*, pp. 1292–1301, Aug. 2004.

[42] K. Sayood and J. C. Brokenhagen, "Use Of Residual Redundancy In The Design Of Joint Source-Channel Coders," *IEEE Trans. on Communications*, pp. 838–846, Jun. 1991.

[43] L. Bahl, J. Cocke, F. Jelinek, J. Raviv, "Optimal Decoding Of Linear Codes For Minimizing Symbol Error Rate," *IEEE Trans. on Information Theory*, pp. 284–287, Mar. 1974.

[44] S. Emami and S. L. Miller, "DPCM Picture Transmission over Noisy Channels with the Aid of a Markov Model," *IEEE Trans. on Image Processing*, pp. 1473–1481, Nov. 1995.

[45] N. Phamdo and F. Alajaji, "Soft-Decision Demodulation Design for COVQ over White, Colored, and ISI Gaussian Channels," *IEEE Trans. on Communications*, pp. 1499–1506, Sep. 2000.

[46] L. Zhao and J. W. Mark, "Mobile Speed Estimation Based on Average Fade Slope Duration," *IEEE Transactions on Communications*, pp. 2066–2069, Dec. 2004.

[47] C. Juncker, P. Toft, and N. Morch, "Speed Estimation for WCDMA based on the Channel Envelope Derivative," *IEEE Workshop on Signal Processing Advances in Wireless Communications (SPAWC)*, pp. 527–531, Jun. 2003.

[48] M. Kirsch and F. Berens, "Mobile Speed Estimation for 3G Mobile Radio Systems using the Normalized Autocovariance Function," *International Zurich Seminar on Broadband Communications*, pp. 48–1–48–4, Feb. 2002.

[49] C. Berrou and A. Glavieux, "Near Optimum Error Correcting Coding and Decoding: Turbo-Codes," *IEEE Trans. on Communications*, pp. 1261–1271, Oct. 1996.

[50] 3GPP Technical Specification, "UMTS Multiplexing and Channel Coding (FDD)," *ETSI TS 125 212 V6.0.0*, Dec. 2003.

[51] Jinho Choi, "Performance Limitation of Closed-Loop Transmit Antenna Diversity over Fast Rayleigh Fading Channels," *IEEE Trans. on Vehicular Technology*, pp. 771–775, Jul. 2002.

[52] B. Raghothaman, G. Mandyam, and R. T. Derryberry, "Performance of Closed-Loop Transmit Diversity with Feedback Delay," *34'th Asilomar Conference*, pp. 102–105, Oct. 2000.

[53] S. Nagaraj and P. Monogioudis, "Antenna verification for closed loop transmit diversity in UMTS," *IEEE Vehicular Technology Conference*, pp. 3792 – 3796, Sep. 2004.

[54] Y. Li, N. B. Mehta, A. F. Molisch, J. Zhang, "Optimal Signaling and Selection Verification for Single Transmit-Antenna Selection," *IEEE Trans. on Communications*, pp. 778–789, Apr. 2007.

[55] A. Heidari, F. Lahouti, D. McAvoy, and A. K. Khandani, "Improvement of Closed-loop Communication Systems in the Presence of Feedback Imperfections," Bell Mobility, Tech. Rep., Dec. 2005.

[56] A. Heidari, D. McAvoy, and A. K. Khandani, "Adaptive Modeling and Long-Range Prediction of Mobile Fading Channels," *submitted to IEEE Transactions on Wireless Communications*, 2007.

[57] ——, "Adaptive Channel Prediction System and Method," Filed Canadian and US Patent Application.

[58] T. Svantesson and A.L. Swindlehurst, "A Performance Bound for Prediction of MIMO Channels," *IEEE Signal Processing Magazine*, pp. 520–529, Feb. 2006.

[59] R.J. Lyman, "Optimal Mean-Square Prediction of the Mobile-Radio Fading Envelope," *IEEE Transactions on Signal Processing*, pp. 819–824, Mar. 2003.

[60] C. Komninakis, C. Fragouli, A.H. Sayed, and R.D. Wesel, "Multi-Input Multi-Output Fading Channel Tracking and Equalization Using Kalman Estimation," *IEEE Transactions on Signal Processing*, pp. 1065–1076, May 2002.

[61] M. Yan and B. D. Rao, "Performance of an Array Receiver with a Kalman Channel Predictor for Fast Rayleigh Flat Fading Environments," *IEEE Journal on selected Areas in Communications*, Jun. 2001.

[62] T. Ekman, G. Kubin, M. Sternad, A. Ahlen, "Quadratic And Linear Filters For Radio Channel Prediction," *IEEE 50th Vehicular Technology Conference (VTC'Fall)*, pp. 146 – 150, Sep. 1999.

[63] J.K. Hwang and J.H Winters, "Sinusoidal Modeling and Prediction of Fast Fading Processes," *IEEE Global Telecommunications Conference (GLOBECOM'98)*, pp. 892–897, Nov. 1998.

[64] J.B. Andersen, J. Jensen, S.H. Jensen, and F. Frederiksen, "Prediction of Future Fading Based on Past Measurements," *IEEE 50th Vehicular Technology Conference (VTC'Fall)*, pp. 151–155, Sep. 1999.

[65] Y. Liu and D. Pang, "Using the Kalman Filter for Long Range Channel Prediction," Master's thesis, Department of Signals and Systems, Chalmers University of Technology, Goteborg, Sweden, Feb. 2005.

[66] M. Chen, M. Viberg, and T. Ekman, "Two New Approaches to Channel Prediction Based on Sinusoidal Modelling," *13th IEEE/SP Workshop on Statistical Signal Processing*, pp. 697–700, Jul. 2005.

[67] S. Haykin, *Adaptive Filter Theory*. Prentice Hall, 1995.

[68] A. Heidari, A. K. Khandani, and D. McAvoy, "Channel Prediction for 3G Communication Systems," Bell Mobility, Tech. Rep., Aug. 2004, available at `http://cst.uwaterloo.ca/~reza`.

[69] A. Papulis, *Probability, Random Variables, and Stochastic Processes*. McGraw-Hill, 1984.

[70] A. Heidari, D. McAvoy, and A. K. Khandani, "Adaptive Long-Range Prediction of Mobile Fading," *The 23rd Biennial Symposium on Communication, Queens University, Kingston, Ontario, Canada*, pp. 219–222, May 2006.

[71] G. Janacek and L. Swift, *Time Series: Forecasting, Simulation, Applications*. Prentice Hall, 1993.

[72] P. A. Matthews and B. Mohebbi, "Direction of Arrival Measurements at UHF," *Electronics Letters*, pp. 1069 – 1070, Aug. 1989.

[73] B. G. Quinn and E. J. Hannan, *The Estimation and Tracking of Frequency*. Cambridge University Press, 2001.

[74] H. Gerlach et al., "Joint Kalman Channel Estimation and Equalization for the UMTS FDD Downlink," *IEEE 58th Vehicular Technology Conference (VTC'Fall)*, pp. 1263–1267, Oct. 2003.

[75] G. H. Golub and C. F. Van Loan, *Matrix Computations*, 3rd ed. Johns Hopkins University Press, 1996.

[76] A. Heidari and A. K. Khandani, "Prediction and Quantization of Givens Rotations for MIMO Channel Precoding," University of Waterloo, Tech. Rep. UW-E&CE #2007-09, Apr. 2007.

[77] M. Ansari, A. K. Khandani, and F. Lahouti, "A New Method of Channel Feedback Quantization for High Data Rate MIMO Systems," *IEEE Trans. on Wireless Communications*, dec 2006.

[78] J. C. Roh and B. D. Rao, "Efficient Feedback Methods for MIMO Channels Based on Parameterization," *IEEE Trans. on Wireless Communications*, pp. 282–293, Jan. 2007.